Synthesis, in vitro cytotoxicity, molecular docking and ADME study of some indolin-2-one linked 1,2,3-triazole derivatives

Synthesis, *invitro* cytotoxicity,molecular docking and ADME study of some indolin-2-one linked 1,2,3-triazole derivatives

Arnika Das[1*], Giulia Greco[2*], Sujeet Kumar[1], Elena Catanzaro[2], Rita Morigi[4], Alessandra Locatelli[4], Dominique Schols[3], Hakan Alici[5], Hakan Tahtaci[6], Febina Ravindran[7], Carmela Fimognari[2**], Subhas S Karki[1**]

[1]Department of Pharmaceutical Chemistry, Dr.Prabhakar B Kore Basic Science Research Centre, Off-Campus, KLECollege of Pharmacy, (A Constituent unit of KAHER-Belagavi), Bengaluru-560010, Karnataka, India
[2]Department for Life Quality Studies, Alma Mater Studiorum – Università di Bologna, Rimini, Italy
[3]Rega Institute for Medical Research, Department of Microbiology, Immunology and Transplantation, Laboratory of Virology and Chemotherapy, KU Leuven, B-3000 Leuven, Belgium
[4]Department of Pharmacy and Biotechnology, Alma Mater Studiorum-Università di Bologna, Italy
[5]Department of Physics,Faculty of Arts and Sciences, Zonguldak Bulent Ecevit University, 67100, Zonguldak, Turkey
[6]Department of Chemistry, Faculty of Science, Karabuk University, 78050, Karabuk, Turkey
[7]Institute of Bioinformatics and Applied Biotechnology, Electronic city phase 1, Bangalore 560100, Karnataka, India

---

*These authors contributed equally to this work.

Corresponding authors: **subhasskarki@gmail.com (Subhas S Karki),

carmela.fimognari@unibo.it (Carmela Fimognari)

Abstract

In pursuit of an anticancer lead, a library of 1,2,3-triazole derivatives (**7a-x)** was prepared, characterized and screened for *invitro* cytotoxicity in different cell lines. Most of the compoundsproved to be cytotoxic withIC_{50}values in the low micromolar range.Furtherstudiesshowed that the most active compound **7c** induces caspase-dependent apoptosis in Jurkat cells by activating both the intrinsic and the extrinsic apoptotic pathways and perturbs cell-cycle progression. Moreover, **7c** did not show any genotoxic activity. Molecular docking simulations were performed against epidermal growth factor receptor (EGFR). Docking experiments showed that, compounds **7c**, **7o** and **7v** bind within active sites of epidermal growth factor receptor EGFR (Pdb ID: 6P8Q) by strong hydrogen bonds with residue *MET793*, Pi-Sulfur with residue *MET790* and Pi-Alkyl type interactions with residues *LEU788*, *ALA743*. The SwissADME webserver investigation suggested that most of the synthesized compounds follow the rules of drug-likeness.

Key words 1,2,3-Triazole, Indolin-2-one, Cytotoxicity,Apoptosis, Cell cycle, Molecular docking, EGFR.

1. Introduction

Resistance to chemotherapy is a main obstacle in cancer treatment. Despite the advances in molecular biology and availability of drug discoverytools, getting a promising anticancer *lead* still seems to be an uphill task. In search of a *lead* with possible anticancer property, the heterocyclic skeletons were explored extensively. Better chemical reactivity, greater receptor affinity, rapid body clearance and low toxicity make heterocyclic moieties the first choice synthon in drug discovery process (Pearce,2017), triazole is an example of it. Further, the development of Disarib (Figure 1) as a potent BCL2-inhibitor (Iyer et al., 2016) paved the idea of synthesizing some indole based triazole analogs with potential anticancer activity. Among heterocycles, indole is one of the most promising moieties. Thanks to its physicochemical properties, indole ring is considered a golden scaffold to design new antitumoral agents (Wan et al., 2019). Indeed, several indole derivatives were reported asanticancer compounds (Wan et al., 2019, Jia et al., 2020), such as Sunitinib, Osimertinib and Nintedanib (**Fig. 1**). 1,2,3-Triazole is a well-known scaffold with substantial biologicalactivities. In fact, 1,2,3-triazole derivatives have been reported as anticancer (Atulya et al., 2016, Chen et al.,2008, Narsimha et al., 2016, Carroux et al., 2013, Duan et al., 2013, Yan et al.,2010, Sztankeet al., 2008), cytotoxic (Das et al., 2021), antioxidant (Mady et al., 2014), anti-HIV (Velázquez et al., 1998, Johns etal., 2009), anti-tubercular (Kumar et al., 2014, Yempala et al., 2014, Patpi et al., 2012), antimicrobial (Hussain et al., 2019, Behbehani et al.,2011, Holla et al., 2005, Chen et al.,2000),antifungal (Sheehan et al.,1999), anti-inflammatory (Hafez et al., 2008, Rao etal., 2014), antimalarial (Gujjar et al., 2009), and anticonvulsant (Ulloora et al., 2013, Erol et al., 1995) agents. Apart from being a versatile synthon, the triazole moiety is used as bioisostere to modify biological and physicochemical properties of a *lead* in drug discovery process (Bonandi et al., 2017). The most common method used to synthesize1,2,3-triazole nucleus is 1,3-dipolar cycloaddition of azide with alkyne (Kumar et al., 2014), and the same has been adopted for the proposed work, which deals with synthesis and *in-vitro* cytotoxicity investigation of newly synthesized 1,2,3-triazole derivatives (**7a-x)**. Moreover, the most active compound **7c** was deeper investigated in order to understandthemolecularmechanisms responsible for its cytotoxic activity.

Further, the pharmacokinetic properties and ADME parameters of the synthesized compounds were also investigated.

Epidermal Growth Factor Receptor (EGFR) is a transmembrane protein regulatingdevelopment and homeostasis; besides, it also plays a key role in cancer development (Sigismund et al., 2018). Indeed, its improper activation, due to gene amplification, mutationsoroverexpression, has been observedin different cancer types, including lung (Mitsudomi et al., 2010), glioblastoma (Verhaak et al., 2010, Mellinghoff et al., 2005), head-neck (Grandis et al., 1998, Kalyankrishna et al., 2006), anal (Walker et al., 2009), and ovarian cancers (Nielsen et al., 2004, Morrison et al., 2012). Therefore, this receptor is assumed to be one of the most important target structures for the development of new anticancer agents (Jain et al., 2018, De Clercq et al., 2019, To et al., 2019).In this context, the crystal structure of EGFR (PDB ID: 6P8Q) was considered as the target structure and the inhibition effect of the synthesized compounds on this receptor was investigated by molecular docking simulations. Here, the calculations were performed with AutoDockVina (Trott et al., 2010) using Lamarckian genetic algorithm (Solis et al., 1981, Huey et al., 2007) and great agreement with *in vitro* results was observed. In addition, the possible binding sites of some high-scoring compounds to EFGR were determined.

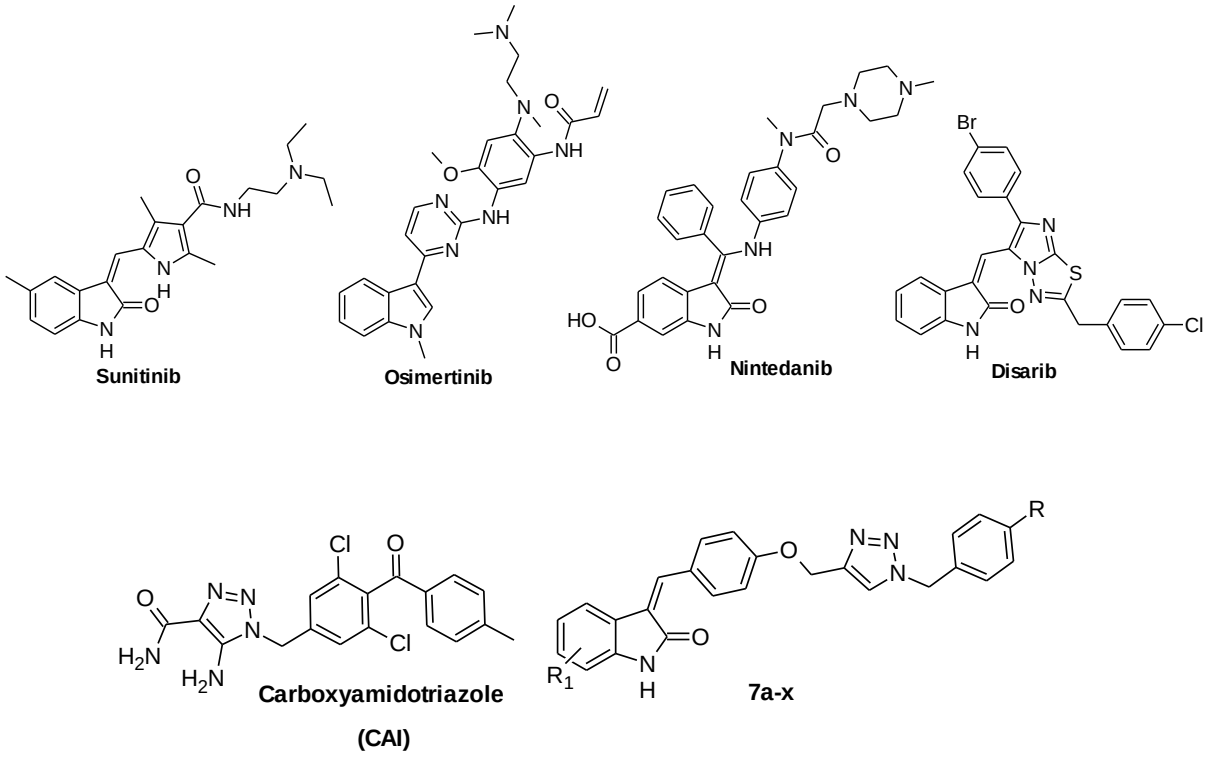

Figure 1. Structures of indole containing drugs (Sunitinib, Osimertinib, Nintedanib and Disarib) in clinical and preclinical stages,triazole containing drug (CAI) and synthesized derivatives **7a-x**.

2. Experimental section

2.1. Chemistry

Reagents and solvents were assured for purity before use. Progress of reactions was confirmed by thin layer chromatography (TLC) on a pre-coated Aluchrosep silica gel 60/UV254 plates (Sd Fine-Chem Ltd.). Melting point (m.p.) was measured by open capillary tube method in liquid paraffin (heavy), and reported uncorrected. Fourier transformer infrared (FTIR) spectra were recorded using infrared (IR) grade potassium bromide (KBr) by diffuse reflectance technique on JASCO 460^{+}. The^{1}H/^{13}C-NMRspectrawere recorded in deuterated dimethyl sulphoxide (DMSO-d_6) and chloroform ($CDCl_3$)between 400-500/100 MHz on Bruker (Ultraspec AMX 400) and JEOL RESONANCE. Chemical shift (δ) values were expressed in ppm using tetramethylsilane (TMS) as reference. CHN analysis was done on thermo scientific Flash 2000 organic elemental analyzer. Mass spectra of (Z)-3-(4-((1-arylmethyl-1H-1,2,3-triazol-4-yl)methoxybenzylidene)indolin-2-ones(**7a-d, 7o** and **7v**) were recorded on triple-quadrupole liquid chromatography mass spectrometry (LC-MS) 6410 from Agilent Technologies. Compounds 4-(prop-2-ynyloxy)benzaldehyde**(3)** and 4-((1-arylmethyl-1*H*-1,2,3-triazol-4-yl)methoxy)benzaldehydes **(5A-D)** were synthesized according to literature (Kumar et al., 2013). Various arylazides **(4A-D)**were prepared as per the literature (Hong et al., 2013). Various indolin-2-ones (6E-J) were prepared according to literature **(**Sorianoet al., 1993). Compounds **7a** and **7s**were prepared as per the literature (Atulya et al., 2016).

2.2. General procedure for the synthesis of (Z)-3-(4-((1-benzyl-1H-1,2,3-triazol-4 yl)methoxy benzylidene)indolin-2-ones(7b-x)

The appropriate aldehyde **5** (1 mmol) was dissolved in anhydrous methanol (30 mL) and treated with the equivalent of respective 2-oxindole **6** and piperidine (0.5 mL). The reaction mixture was refluxed and the precipitate formed on cooling was collected by filtration and recrystallized from DMF/methanol mixture in various proportions.

2.2.1. *(Z)-3-(4-((1-benzyl-1H-1,2,3-triazol-4-yl)methoxy)benzylidene)-5-chloroindolin -2-one (7b)*

Yield 58%; m.p.260-262 °C; IR (KBr) ν_{max}/cm^{-1}: 3204, 3050, 2945, 1697, 1590, 1511, 1464, 1185;^{1}H-NMR (400 MHz, DMSO-d_6, δ/ppm)**:** 10.71 (s, 1H, -NH), 8.50 (d, 2H, J=7.2 Hz), 8.32 (s, 1H, triazole-H), 7.88 (s, 1H, benzylidene-H), 7.81-7.80 (d, 1H, J=2.0 Hz), 7.39-7.36 (m, 2H, ar.), 7.34-7.31 (m, 3H, ar.), 7.21-7.19 (m, 1H, ar.), 7.15 (d, 2H, J=7.2 Hz), 6.81 (d, 1H, J=6.4 Hz), 5.61 (s, 2H, -OCH_2-), 5.24 (s, 2H, -NCH_2-). ^{13}C-NMR (100 MHz, DMSO-d_6, δ/ppm): 167.09, 160.27, 142.54, 138.84, 138.68, 135.93, 134.70, 128.73, 128.12, 127.92, 127.55, 127.27, 127.06, 125.24, 124.82, 123.03, 119.28, 114.53, 110.49, 61.20, 52.82.Anal. Calcd. for $C_{25}H_{19}ClN_4O_2$: C, 67.80; H, 4.32; N, 12.65: Found C, 67.67; H, 4.25; N, 12.69%. +MS (ESI) m/z: 443.20 (442.90).

2.2.2. *(Z)-3-(4-((1-benzyl-1H-1,2,3-triazol-4-yl)methoxy)benzylidene)-5-methylindolin -2-one (7c)*

Yield 55%; m.p.220-222°C; IR (KBr) ν_{max}/cm^{-1}:3198, 3049, 2876, 1698, 1601, 1543, 1482, 1379, 1201; ^{1}H-NMR (400 MHz, DMSO-d_6, δ/ppm)**:** 10.44 (s, 1H,-NH), 8.47 (d, 2H, J=9.2 Hz), 8.37 (s, 1H, triazole-H), 7.69 (s, 1H, benzylidene-H),7.49 (s, 1H, ar.), 7.40-7.31 (m, 5H, ar.), 7.13 (d, 2H, J=8.8 Hz), 6.99 (d, 1H, J=8.4 Hz), 6.70 (d, 1H, J=7.6 Hz), 5.61 (s, 2H,-OCH_2-), 5.23 (s, 2H, -NCH_2-), 2.29 (s, 3H, -CH_3). ^{13}C-NMR (100 MHz, DMSO-d_6, δ/ppm): 167.45, 159.22, 142.66, 140.40, 136.31, 135.95, 135.57, 134.28, 131.41, 130.12,

129.61, 128.74, 128.14, 127.93, 126.95, 125.90, 124.80, 122.59, 119.74, 114.92, 114.42, 109.73, 108.91, 61.22, 52.84. Anal. Calcd. for $C_{25}H_{22}N_4O_2$: C, 73.92; H, 5.25; N, 13.26: Found C, 73.81; H, 5.21; N, 13.23%. +MS (ESI) m/z: 423.2 (422.48).

2.2.3. ***(Z)-3-(4-((1-benzyl-1H-1,2,3-triazol-4-yl)methoxy)benzylidene)-5-bromoindolin--2-one (7d)***

Yield 62%; m.p.238-240°C; IR (KBr) ν_{max}/cm^{-1}:3154, 3038, 2941 1697, 1591, 1512, 1471, 1186; ^{1}H-NMR (400 MHz, DMSO-d_6, δ/ppm): 10.72 (s, 1H, -NH), 8.50 (d, 2H, J=6.8 Hz) 8.32 (s, 1H, triazole-H), 7.93 (s, 1H, ar.), 7.89 (s, 1H, benzylidene-H), 7.70-7.65 (m, 1H, ar.),7.40-7.31 (m, 5H, ar.), 7.22-7.13 (m, 2H, ar.), 6.84-6.75 (m, 1H, ar.) 5.61 (s, 2H, -OCH_2-), 5.24 (s, 2H, -NCH_2-). Anal. Calcd. for $C_{25}H_{19}BrN_4O_2$: C, 61.61; H, 3.93; N, 11.50: Found C, 61.53; H, 3.95; N, 11.53%. -MS (ESI) m/z: 485.0 (487.35).

2.2.4. ***(Z)-3-(4-((1-benzyl-1H-1,2,3-triazol-4-yl)methoxy)benzylidene)-7-chloroindolin -2-one (7e)***

Yield 73%;m.p.214-216 °C; IR (KBr) ν_{max}/cm^{-1}:3151, 3040, 2925, 1700, 1592, 1449, 1482, 1226; ^{1}H-NMR (400 MHz, DMSO-d_6, δ/ppm): 10.99 (s, 1H, -NH), 8.49 (d, 2H, J=9.2 Hz), 8.31 (s, 1H, triazole-H), 7.83 (s, 1H, benzylidene-H), 7.67 (d, 1H, J=7.2 Hz), 7.40-7.28 (m, 5H, ar.), 7.25 (d, 1H, J=8.8 Hz), 7.16 (d, 2H, J=8.8 Hz), 7.00 (t, 1H, J=15.6 Hz), 5.61 (s, 2H, -OCH_2-), 5.24 (s, 2H, -NCH_2-).^{13}C-NMR (100 MHz, DMSO-d_6, δ/ppm): 167.22, 160.31, 142.56, 138.75, 137.49, 135.94, 134.69, 128.75, 128.14, 127.94, 127.71, 127.19, 126.99, 124.84, 123.49, 122.06, 117.85, 114.55, 113.54, 61.22, 52.84. Anal. Calcd. for $C_{25}H_{19}ClN_4O_2$: C, 67.80; H, 4.32; N, 12.65: Found C, 67.71; H, 4.35; N, 12.66%.

2.2.5. ***(Z)-3-(4-((1-benzyl-1H-1,2,3-triazol-4-yl)methoxy)benzylidene)-6-chloroindolin--2-one (7f)***

Yield 65%;m.p.181-183°C; IR (KBr) ν_{max}/cm^{-1}:3198, 3030, 2845, 1698, 1604, 1543, 1476, 1184; ^{1}H-NMR (500 MHz, DMSO-d_6, δ/ppm)**:** 10.86 (s, 1H, -NH), 8.41 (s, 1H, triazole-H), 8.32-8.29 (m, 3H, ar.), 7.39-7.36 (m, 2H, ar.), 7.34-7.31(m, 3H, ar.), 7.19 (t, 1H, J=12.8 Hz), 7.12 (d, 2H, J=7.2 Hz), 7.01 (d, 1H, J=7.2 Hz), 6.81 (d, 1H, J=6.8 Hz), 5.61 (s, 2H, -OCH_2-), 5.24 (s, 2H, -NCH_2-).^{13}C-NMR (100 MHz, DMSO-d_6, δ/ppm): 167.09, 160.27, 142.54, 138.84, 138.68, 135.93, 134.70, 128.72, 128.12, 127.92, 127.54, 127.26, 127.06, 125.24, 124.82, 123.03, 119.28, 114.52, 110.48, 61.20, 52.82.Anal. Calcd. for $C_{25}H_{19}ClN_4O_2$: C, 67.80; H, 4.32; N, 12.65: Found C, 67.68; H, 4.29; N, 12.69%.

2.2.6. ***(Z)-5-chloro-3-(4-((1-(4-nitrobenzyl)1H-1,2,3-triazol-4-yl)methoxy) benzylidene)indolin-2-one (7g)***

Yield 55%; m.p.220-222°C; IR (KBr) ν_{max}/cm^{-1}:3201, 3060, 2890, 1701, 1599, 1560, 1512, 1483, 1192; ^{1}H-NMR (400 MHz, DMSO-d_6, δ/ppm): 10.69 (s, 1H, -NH), 8.50 (d, 2H, J=8.8 Hz), 8.39 (s, 1H, triazole-H), 8.25 (d, 2H, J=8.8 Hz), 7.88 (s, 1H, benzylidene-H), 7.80-7.79 (m, 1H, ar.), 7.55 (d, 2H, J=8.8 Hz), 7.21-7.18 (m, 1H, ar.), 7.15 (d, 2H, J=8.8 Hz), 6.82 (d, 1H, J=8.0 Hz), 5.80 (s, 2H, -OCH_2-), 5.27 (s, 2H, -NCH_2-).^{13}C-NMR (100 MHz, DMSO-d_6, δ/ppm): 167.12, 160.24, 147.25, 143.32, 142.76, 138.87, 138.66, 134.72, 129.04, 127.59, 127.28, 127.13, 125.28, 123.90, 123.11, 119.31, 114.59, 110.52, 61.20, 51.95. Anal. Calcd. for $C_{25}H_{18}ClN_5O_4$: C, 61.54; H, 3.72; N, 14.35: Found C, 61.45; H, 3.67; N, 14.39%.

2.2.7. ***(Z)-5-bromo-3-(4-((1-(4-nitrobenzyl)-1H-1,2,3-triazol-4-yl)methoxy) benzylidene)indolin-2-one (7h)***

Yield 65%; m.p.210-212°C; IR (KBr) ν_{max}/cm^{-1}:3157, 3078, 2856, 1698, 1589, 1477, 1190; ^{1}H-NMR (400 MHz, DMSO-d$_6$, δ/ppm)**:** 10.70 (s, 1H, -NH), 8.50 (d, 2H, J=9.2 Hz), 8.39 (s, 1H, triazole-H), 8.25 (d ,2H, J=8.8 Hz), 7.92 (m, 2H, ar.), 7.54 (d, 2H, J=8.8 Hz), 7.34-7.31 (m, 1H, ar.), 7.16 (d, 2H, J=9.2 Hz), 6.77 (d, 1H, J=8.4 Hz), 5.80 (s, 2H, -OCH$_2$-), 5.27 (s, 2H, -NCH$_2$-).^{13}C-NMR (100 MHz, DMSO-d$_6$, δ/ppm): 166.98, 160.23, 147.25, 143.32, 142.75, 139.22, 138.68, 134.72, 130.37, 129.03, 127.70, 127.13, 125.27, 123.89, 122.94, 122.03, 114.57, 112.94, 111.02, 61.19, 51.93. Anal. Calcd. for $C_{25}H_{18}BrN_5O_4$: C, 56.41; H, 3.41; N, 13.16: Found C, 56.37; H, 3.35; N, 13.20%.

2.2.8. ***(Z)-6-chloro-3-(4-((1-(4-nitrobenzyl)-1H-1,2,3-triazol-4-yl)methoxy) benzylidene)indolin-2-one (7i)***

Yield 54%; m.p.178-180°C;IR (KBr) ν_{max}/cm^{-1}:3201, 3090, 2864, 1695, 1616, 1528, 1499, 1472, 1185; ^{1}H-NMR (500 MHz, DMSO-d$_6$, δ/ppm): 10.86 (s, 1H, -NH), 8.41 (d, 2H, J=6.0 Hz), 8.32 (d, 2H, J=6.8 Hz), 8.25-8.21 (m, 2H, ar.), 7.54 (d, 2H, J=7.2 Hz), 7.19 (t, 1H, J=12.8 Hz), 7.12 (d, 2H, J=7.2 Hz), 7.01 (d, 1H, J=6.8 Hz), 6.81 (d, 1H, J=6.8 Hz), 5.81 (s, 2H, -OCH$_2$-), 5.26 (s, 2H, -NCH$_2$-).^{13}C-NMR (100 MHz, DMSO-d$_6$, δ/ppm): 167.19, 159.41, 143.31, 136.74, 134.51, 131.60, 129.00, 126.70, 125.24, 123.88, 123.24, 120.73, 120.03, 115.09, 114.53, 109.92, 61.13, 51.92. Anal. Calcd. for $C_{25}H_{18}ClN_5O_4$: C, 61.54; H, 3.72; N, 14.35: Found C, 61.49; H, 3.65; N, 14.41%.

2.2.9. ***(Z)-7-chloro-3-(4-((1-(4-nitrobenzyl)-1H-1,2,3-triazol-4-yl)methoxy) benzylidene)indolin-2-one (7j)***

Yield 58%; m.p.210-213°C; IR (KBr) ν_{max}/cm^{-1}:3227, 3066, 2950, 1695, 1610, 1514, 1481, 1432, 1174; ^{1}H-NMR (400 MHz, DMSO-d$_6$, δ/ppm)**:** 11.00 (s, 1H, -NH), 8.50 (d, 2H, J=9.2 Hz), 8.39 (s, 1H, triazole-H), 8.25-8.22 (d, 2H, J=8.8 Hz), 7.84 (s, 1H, benzylidene-H), 7.67 (d, 1H, J=7.6 Hz), 7.55-7.52 (d, 2H, J=8.8 Hz), 7.23 (d, 1H, J=8.8 Hz), 7.17 (d, 2H, J=8.8 Hz), 6.99 (t, 1H, J=15.6 Hz), 5.81 (s, 2H, -OCH$_2$-), 5.27 (s, 2H, -NCH$_2$-).^{13}C-NMR (100 MHz, DMSO-d$_6$, δ/ppm): 167.22, 160.26, 147.25, 143.32, 142.75, 138.71, 137.50, 134.69, 129.04, 127.72, 127.19, 127.03, 125.28, 123.53, 122.06, 117.86, 114.58, 113.55, 61.20, 51.94. Anal. Calcd. for $C_{25}H_{18}ClN_5O_4$: C, 61.54; H, 3.72; N, 14.35: Found C, 61.42; H, 3.61; N, 14.44%.

2.2.10. ***(Z)-3-(4-((1-(4-nitrobenzyl)-1H-1,2,3-triazol-4-yl)methoxy)benzylidene)indolin -2-one (7k)***

Yield 63%; m.p.214-215°C; IR (KBr) ν_{max}/cm^{-1}:3247, 3059, 2919, 1695, 1610, 1514, 1449, 1481, 1174; ^{1}H-NMR (400 MHz, DMSO-d$_6$, δ/ppm)**:** 10.56 (s, 1H, -NH), 8.48 (d, 2H, J=8.8 Hz), 8.38 (s, 1H, triazole-H), 8.23 (d, 2H, J=8.8 Hz), 7.94-7.52 (sdd, 4H, J=8.8 Hz, 8.8 Hz), 7.23-7.12 (td, 3H, J=15.6 Hz, 8.4 Hz), 6.96 (t, 1H, J=16 Hz), 6.81 (d, 1H, J=8.0 Hz), 5.80 (s, 2H, -OCH$_2$-) 5.26 (s, 2H, -NCH$_2$-).^{13}C-NMR (100 MHz, DMSO-d$_6$, δ/ppm): 167.32, 159.81, 147.23, 143.31, 142.81, 140.25, 136.61, 134.31, 129.01, 128.23, 127.28, 125.27, 125.23, 124.23, 123.88, 120.85, 119.23, 114.44, 109.15, 61.15, 51.92. Anal. Calcd. for $C_{25}H_{19}N_5O_4$: C, 66.22; H, 4.22; N, 15.44: Found C, 66.15; H, 4.16; N, 15.49%.

2.2.11. ***(Z)-5-methyl-3-(4-((1-(4-nitrobenzyl)-1H-1,2,3-triazol-4-yl)methoxy)- benzylidene)indolin-2-one (7l)***

Yield 55%; m.p.216-218°C; IR (KBr) ν_{max}/cm^{-1}:3169, 3010, 2826, 1672, 1602, 1594, 1503, 1489, 1376, 1189. ^{1}H-NMR (400 MHz, DMSO-d$_6$, δ/ppm): 10.41 (s, 1H, -NH), 8.39 (s, 1H, triazole-H), 8.24 (d, 2H, J=8.8 Hz), 7.71 (d, 2H, J=8.8 Hz), 7.55-7.52 (m, 3H, ar.), 7.44 (s, 1H, ar.), 7.20 (d, 2H, J=8.8 Hz), 7.03 (d, 1H, J=7.2 Hz), 6.76 (d, 1H, J=8.0 Hz), 5.81 (s, 2H,-OCH$_2$-), 5.29 (s, 2H, -NCH$_2$-), 2.17 (s, 3H, -CH$_3$). ^{13}C-NMR (100 MHz, DMSO-d$_6$,

δ/ppm): 168.90, 159.16, 147.22, 143.31, 142.84, 140.40, 135.51, 134.27, 131.39, 130.11, 129.56, 127.00, 125.93 (s), 125.21, 123.88, 122.56, 121.16, 114.94, 109.71, 61.21, 51.92, 20.79. Anal. Calcd. for $C_{26}H_{21}N_5O_4$: C, 66.80; H, 4.53; N, 14.98: Found C, 66.59; H, 4.48; N, 15.01%.

2.2.12. ***(Z)-3-(4-((1-(4-methylbenzyl)-1H-1,2,3-triazol-4-yl)methoxy)benzylidene) indolin-2-one (7m)***

Yield 70%; m.p.200-201°C; IR (KBr) ν_{max}/cm^{-1}:3229, 3010, 2811, 1692, 1594, 1498, 1476, 1386, 1167; ^{1}H-NMR (500 MHz, DMSO-d$_6$, δ/ppm)**:** 10.58 (s, 1H,-NH), 8.47 (d, 2H, J=7.2 Hz), 8.28 (s, 1H, triazole-H), 7.74 (s, 1H, benzylidene-H), 7.67 (d, 1H, J=6.0 Hz), 7.22 (m, 2H, ar.), 7.18 (m, 3H, ar.), 7.13 (d, 2H, J=7.2 Hz), 6.97 (t, 1H, J=13.2 Hz), 6.81 (d, 1H, J=6.0 Hz), 5.55 (s, 2H, -OCH$_2$-), 5.22 (s, 2H -NCH$_2$-), 2.67 (s, 3H, -CH$_3$).^{13}C-NMR (100 MHz, DMSO-d$_6$, δ/ppm): 167.33, 159.87, 142.58, 140.24, 137.49, 136.67, 134.32, 132.94, 129.27, 128.24, 127.98, 127.25, 125.29, 124.65, 124.18, 120.87, 119.24, 114.44, 109.16, 61.18, 52.64, 20.64.Anal. Calcd. for $C_{25}H_{22}N_4O_2$: C, 73.92; H, 5.25; N, 13.26: Found C, 73.81; H, 5.21; N, 13.32%.

2.2.13. ***(Z)-6-chloro-3-(4-((1-(4-methylbenzyl)-1H-1,2,3-triazol-4-yl)methoxy) benzylidene)indolin-2-one (7n)***

Yield 56%; m.p.189-190°C;IR (KBr) ν_{max}/cm^{-1}:3203, 3023, 2838, 1692, 1586, 1509 , 1448, 1389, 1175; ^{1}H-NMR (500 MHz, DMSO-d$_6$, δ/ppm): 10.86 (s, 1H, -NH), 8.40 (s, 1H, ar.), 8.32 (d, 2H, J=7.2 Hz), 8.27 (s, 1H, triazole-H), 7.22-7.20 (m, 2H, ar.), 7.19-7.16 (m, 3H, ar.), 7.11 (d, 2H, J=7.2 Hz), 7.01 (d, 1H, J=7.2 Hz), 6.81 (d, 1H, J=7.2 Hz), 5.55 (s, 2H, -OCH$_2$-), 5.22 (s, 2H, -NCH$_2$-), 2.27 (s, 3H, -CH$_3$).^{13}C-NMR (100 MHz, DMSO-d$_6$, δ/ppm): 167.20, 160.13, 142.53, 141.31, 137.82, 137.49, 134.52, 132.93, 132.24, 129.26, 127.98, 127.08, 124.66, 124.29, 122.98, 120.67, 120.64, 114.51, 109.12, 61.20, 52.64, 20.64.Anal. Calcd. for $C_{26}H_{21}ClN_4O_2$: C, 68.34; H, 4.63; N, 12.26: Found C, 68.25; H, 4.57; N, 12.31%.

2.2.14. ***(Z)-5-methyl-3-(4-((1-(4-methylbenzyl)-1H-1,2,3-triazol-4-yl)methoxy) benzylidene)indolin-2-one (7o)***

Yield 60%; m.p.208-210°C; IR (KBr) ν_{max}/cm^{-1}:3198, 3043, 2821, 1695, 1602, 1528, 1489, 1378, 1184; ^{1}H-NMR (400 MHz, DMSO-d$_6$, δ/ppm)**:** 10.41 (s, 1H, -NH), 8.27 (s, 1H, triazole-H), 7.70 (d, 2H, J=8.8 Hz), 7.53 (s, 1H, benzylidene-H), 7.45 (s, 1H, ar), 7.23-7.16 (m, 6H, ar.), 7.04 (d, 1H, J=8.0 Hz), 6.76 (d, 1H, J=8.0 Hz), 5.55 (s, 2H, -OCH$_2$-), 5.22 (s, 2H, -NCH$_2$-), 2.27 (s, 3H, -CH$_3$), 2.18 (s, 3H, -CH$_3$). + MS (ESI) m/z: 437.50 (436.52).^{13}C-NMR (100 MHz, DMSO-d$_6$, δ/ppm): 167.44, 159.79, 142.62, 138.02, 136.30, 135.94, 134.27, 129.60, 128.73, 128.66, 128.12, 127.92, 127.31, 125.34, 124.79, 124.38, 119.73, 114.41, 108.90, 61.16, 52.82, 20.78.Anal. Calcd. for $C_{27}H_{24}N_4O_2$: C, 74.29; H, 5.54; N, 12.84: Found C, 74.15; H, 5.47; N, 12.91%.

2.2.15. ***(Z)-5-bromo-3-(4-((1-(4-methylbenzyl)-1H-1,2,3-triazol-4-yl)methoxy) benzylidene)indolin-2-one (7p)***

Yield 46%; m.p.238-240°C; IR (KBr) ν_{max}/cm^{-1}:3158, 3043, 2859, 1698, 1611, 1512, 1462, 1381, 1187; ^{1}H-NMR (400 MHz, DMSO-d$_6$, δ/ppm): 10.70 (s, 1H,-NH), 8.50 (d, 2H, J=9.2 Hz), 8.27 (s, 1H, triazole H), 7.92 (d, 1H, J=2.0, ind4), 7.88 (s, 1H, benzylidene-H), 7.34-7.31 (dd, 1H, J=8.4, ind6), 7.23-7.12 (m, 6H, ar.), 6.77 (d, 1H, J=8.0 Hz), 5.55 (s, 2H, -OCH$_2$-) 5.23 (s, 2H, -NCH$_2$-), 2.27 (s, 3H, -CH$_3$).^{13}C-NMR (100 MHz, DMSO-d$_6$, δ/ppm): 166.96, 160.28, 142.50, 139.20, 138.71, 137.47, 134.71, 132.92, 130.34, 129.25, 127.97, 127.70, 127.07, 124.66, 122.88, 122.01, 114.53, 112.93, 111.00, 61.20, 52.63, 20.63.Anal. Calcd. for $C_{26}H_{21}BrN_4O_2$: C, 62.28; H, 4.22; N, 11.17: Found C, 62.16; H, 4.17; N, 11.21%.

2.2.16. ***(Z)-5-chloro-3-(4-((1-(4-methylbenzyl)-1H-1,2,3-triazol-4-yl)methoxy) benzylidene)indolin-2-one (7q)***

Yield 48%; m.p.242-244°C; IR (KBr) ν_{max}/cm^{-1}:3158, 3059, 2890, 1699, 1590, 1510, 1465, 1381, 1187; ^{1}H-NMR (400 MHz, DMSO-d$_6$, δ/ppm): 10.69 (s, 1H,-NH), 8.49 (d, 2H, J=8.8 Hz), 8.27 (s, 1H, triazole-H), 7.88-7.80 (m, 2H, ar.), 7.23-7.12 (m, 7H, ar.), 6.77 (d, 1H, J=8.4 Hz), 5.55 (s, 2H, -OCH$_2$-), 5.23 (s, 2H, -NCH$_2$-), 2.26 (s, 3H, -CH$_3$).^{13}C-NMR (100 MHz, DMSO-d$_6$, δ/ppm): 167.09, 160.27, 142.50, 138.84, 138.68, 137.47, 134.70, 132.92, 131.52, 129.23, 127.96, 127.54, 127.27, 127.06, 125.24, 124.66, 123.03, 119.27, 114.53, 110.48, 61.20, 52.63, 20.63.Anal. Calcd. for $C_{26}H_{21}ClN_4O_2$: C, 68.34; H, 4.63; N, 12.26: Found C, 68.27; H, 4.53; N, 12.23%.

2.2.17. ***(Z)-7-chloro-3-(4-((1-(4-methylbenzyl)-1H-1,2,3-triazol-4-yl)methoxy) benzylidene)indolin-2-one (7r)***

Yield 55%; m.p.212-214°C; IR (KBr) ν_{max}/cm^{-1}:3201, 3023, 2804, 1698, 1612, 1554, 1486, 1379, 1198; ^{1}H-NMR (400 MHz, DMSO-d$_6$, δ/ppm): 11.00 (s, 1H, -NH), 8.49 (d, 2H, J=8.8 Hz), 8.27 (s, 1H, triazole-H), 7.84 (s, 1H, benzylidene-H), 7.67 (d, 1H, J=7.2 Hz), 7.25-7.13 (m, 7H, ar.), 6.99 (t, 1H, J=15.6 Hz), 5.50 (s, 2H, -OCH$_2$-), 5.23 (s, 2H, -NCH$_2$-), 2.27 (s, 3H, -CH$_3$).^{13}C-NMR (100 MHz, DMSO-d$_6$, δ/ppm): 167.22, 160.30, 142.52, 138.74, 137.49, 134.69, 132.93, 129.26, 127.98, 127.70, 127.19, 126.99, 124.68, 123.48, 122.05, 117.84, 114.55, 113.54, 61.22, 52.65, 20.64.Anal. Calcd. for $C_{26}H_{21}ClN_4O_2$: C, 68.34; H, 4.63; N, 12.26: Found C, 68.24; H, 4.57; N, 12.32%.

2.2.18. ***(Z)-5-chloro-3-(4-((1-(4-chlorobenzyl)-1H-1,2,3-triazol-4-yl)methoxy) benzylidene)indolin-2-one (7t)***

Yield 52%; m.p.242-244°C; IR (KBr) ν_{max}/cm^{-1}:3201, 3051, 2862, 1701, 1623, 1545, 1486, 1201; ^{1}H-NMR (500 MHz, DMSO-d$_6$, δ/ppm): 10.77 (s, 1H, -NH), 8.55 (d, 2H, J=8.8), 8.32 (s, 1H, triazole-H), 7.92 (s, 1H, benzylidene-H), 7.82 (m, 1H, ar.), 7.43 (d, 2H, J=8.2 Hz), 7.38 (d, 2H, J=8.2 Hz), 7.26-7.22 (m, 1H, ar.), 7.18 (d, 2H, J=8.8 Hz), 6.82 (d, 1H, J=8.8 Hz), 5.63 (s, 2H, -OCH$_2$-), 5.26 (s, 2H, -NCH$_2$-). ^{13}C-NMR (100 MHz, DMSO-d$_6$, δ/ppm): 167.09, 160.24, 142.60, 138.84, 138.67, 134.92, 134.70, 129.87, 128.73, 127.55, 127.26, 127.08, 125.24, 124.87, 123.05, 119.28, 114.54, 110.49, 61.19, 52.00. Anal. Calcd. for $C_{25}H_{18}Cl_2N_4O_2$: C, 62.91; H, 3.80; N, 11.74: Found C, 63.01; H, 3.71; N, 11.79%.

2.2.18.1. (Z)-5-bromo-3-(4-((1-(4-chlorobenzyl)-1H-1,2,3-triazol-4-yl)methoxy) benzylidene)indolin-2-one (7u)

Yield 67%; m.p.242-243°C; IR (KBr) ν_{max}/cm^{-1}:3204, 3013, 2798, 1695, 1613, 1542, 1486, 1198; ^{1}H-NMR (500 MHz, DMSO-d$_6$, δ/ppm): 10.73 (s, 1H, -NH), 8.50 (d, 2H, J=8.8 Hz), 8.33 (s, 1H, triazole-H), 7.93 (s, 1H, benzylidene-H), 7.89 (s, 1H, ar.), 7.45 (d, 2H, J=8.0 Hz), 7.35-7.31 (m, 3 H, ar.), 7.15 (d, 2H, J=8.0 Hz), 6.77 (d, 1H, J=8.0 Hz), 5.62 (s, 2H, -OCH$_2$-), 5.24 (s, 2H, -NCH$_2$-).^{13}C-NMR (100 MHz, DMSO-d$_6$, δ/ppm): 166.99, 160.27, 142.63, 139.22, 138.72, 134.93, 134.74, 132.88, 130.38, 129.90, 128.76, 127.71, 127.11, 124.90, 122.92, 122.03, 114.57, 112.96, 111.04, 61.21, 52.04. Anal. Calcd. for $C_{25}H_{18}BrClN_4O_2$: C, 57.55; H, 3.48; N, 10.74: Found C, 57.48; H, 3.45; N, 10.82%.

2.2.19. ***(Z)-3-(4-((1-(4-chlorobenzyl)-1H-1,2,3-triazol-4-yl)methoxy)benzylidene)-5 methylindolin-2-one (7v)***

Yield 56%; m.p.220-221°C; IR (KBr) ν_{max}/cm^{-1}:3141, 3030, 2911, 1682, 1582, 1520, 1482, 1380, 1173; ^{1}H-NMR (500 MHz, DMSO-d$_6$, δ/ppm): 10.48 (s, 1H,-NH), 8.46 (d, 2H, J=8.0), 8.34 (s, 1H, triazole-H), 7.70 (s, 1H, benzylidene-H), 7.49 (s, 1H, ar.), 7.45 (d, 2H,

J=8.0 Hz),7.35 (d, 2H, J=8.0 Hz), 7.11 (d, 2H, J=8.2 Hz), 6.97 (d, 1H, J=8.2 Hz), 6.68 (d, 1H, J=8.0 Hz), 5.62 (s, 2H, -OCH_2-), 5.22 (s, 2H, -NCH_2-), 2.29 (s, 3H, -CH_3).^{13}C-NMR (100 MHz, DMSO-d_6, δ/ppm): 167.44, 159.77, 142.69, 138.03, 136.28, 134.92, 134.27, 131.40, 129.88, 128.73, 127.33, 126.97, 125.33, 124.85, 124.40, 119.73, 114.42, 108.90, 61.15, 52.01, 20.78.Anal. Calcd. for $C_{26}H_{21}ClN_4O_2$: C, 68.34; H, 4.63; N, 12.26: Found C, 68.25; H, 4.55; N, 12.36%. + MS (ESI) m/z: 457.50 (456.93).

2.2.20. ***(Z)-6-chloro-3-(4-((1-(4-chlorobenzyl)-1H-1,2,3-triazol-4-yl)methoxy) benzylidene)indolin-2-one (7w)***

Yield 68%; m.p.242-246°C; IR (KBr) ν_{max}/cm^{-1}:3142, 3042, 2828, 1700, 1613, 1511, 1476, 1176; ^{1}H-NMR (500 MHz, DMSO-d_6, δ/ppm): 10.75 (s, 1H, -NH), 8.47 (d, 2H, J=8.0), 8.33 (s, 1H, triazole-H), 7.80 (s, 1H, benzylidene-H), 7.70 (d, 2H, J=8.0 Hz), 7.45 (d, 2H, J=8.0 Hz), 7.35 (d, 2H, J=8.0 Hz), 7.14 (d, 2H, J=8.0 Hz), 6.82 (d, 1H, J=8.0 Hz), 5.62 (s, 2H, -OCH_2-), 5.23 (s, 2H, -NCH_2-).^{13}C-NMR (100 MHz, DMSO-d_6, δ/ppm): 168.80, 159.45, 143.97, 142.67, 136.79, 134.93, 133.61, 132.88, 131.58, 129.89, 128.74, 126.68, 124.87, 124.59, 123.26, 120.77, 120.05, 115.07, 109.94, 61.24, 52.03. Anal. Calcd. for $C_{25}H_{18}Cl_2N_4O_2$: C, 62.91; H, 3.80; N, 11.74: Found C, 62.83; H, 3.69; N, 11.83%.

2.2.21. ***(Z)-7-chloro-3-(4-((1-(4-chlorobenzyl)-1H-1,2,3-triazol-4-yl)methoxy) benzylidene)indolin-2-one (7x)***

Yield 62%; m.p.250-252°C; IR (KBr) ν_{max}/cm^{-1}: 3201, 3015, 2811, 1699, 1604, 1548, 1486, 1201; ^{1}H-NMR (500 MHz, DMSO-d_6, δ/ppm): 11.04 (s, 1H, -NH), 8.50 (d, 2H, J=8.0 Hz), 8.33 (s, 1H, triazole-H), 7.85 (s, 1H, benzylidene-H), 7.68 (s, 1H, ar.), 7.45 (d, 2H, J=8.0 Hz), 7.35 (d, 2H, J=8.0 Hz), 7.23 (m, 1H, ar), 7.16 (d, 2H, J=8.0 Hz), 7.00 (t, 1H, J=16.0 Hz), 5.62 (s, 2H, -OCH_2-), 5.24 (s, 2H, -NCH_2-). ^{13}C-NMR (100 MHz, DMSO-d_6, δ/ppm): 167.21, 160.27, 142.62, 138.70, 137.49, 134.91, 134.68, 132.88, 131.68, 129.88, 128.73, 127.69, 127.18, 127.00, 124.88, 123.50, 122.03, 117.83, 115.04, 114.54, 113.54, 61.21, 52.03. Anal. Calcd. for $C_{25}H_{18}Cl_2N_4O_2$: C, 62.91; H, 3.80; N, 11.74: Found C, 62.83; H, 3.74; N, 11.81%.

2.3.Cell cultures and Treatments

Human T-lymphoblastic cells (Jurkat and CEM) and human acute promyelocytic cells (HL-60) were provided from LGC standards (LGC Group, Middlesex, UK). Jurkat and CEM cells were cultured in Roswell Park Memorial Institute (RPMI) 1640 medium supplemented with 10% heat-inactivated bovine serum, 1% penicillin/streptomycin solution, and 1% l-glutamine solution (all obtained from Sigma Aldrich). HL-60 cells were cultured in RPMI 1640 supplemented with 20% heat-inactivated bovine serum, 1% penicillin/streptomycin solution, and 1% l-glutamine solution (all obtained from Sigma Aldrich). 293T (human embryonic kidney epithelial cell line was purchased from National Centre for Cell Science, Pune, India. Cells were maintained at 37°C and 5% CO_2 in a humidified atmosphere.Cells were treated with increasing concentrations of the 1,2,3-traizole analog **(7c)** for different time pointsdepending on the biological assay. Etoposide 10µg/mL, camptothecin 2µM, and H_2O_2 0.5 and 1mM (all obtained from Sigma Aldrich) were used as positive controls.

To evaluate the induction of non-canonical cell death pathways, cells were pre-treated for 1h with different chemical inhibitors and then treated with **7c** 8µM for 24 or 48h. For this purpose, the following blockers were used: the pan-caspase inhibitor carbobenzoxy-valyl-alanyl-aspartyl-[O-methyl]-fluoromethylketone (Z-VAD-FMK; BioVision, CA, USA) 75µM; the PARP-1/-2 inhibitor olaparib (Ola; Selleckem, Houston, TX, USA) 5µM; the RIP1 inhibitor II 7-Cl-O-Nec-1 or necrostatin-1s (Nec-1s; Sigma Aldrich) 75µM; the inhibitor of ROS generation and lipid peroxidation ferrostatin-1 (Ferr-1, Sigma Aldrich) 1µM; the iron

chelator deferoxamine mesylate (DFO, Across Organics, Thermofisher Scientific, MA, USA) 10μM and the peroxyl radical scavenger vitamin E (Vit E, Sigma Aldrich) 100μM, in order to inhibit apoptosis, parthanatos, necroptosis and ferroptosis, respectively.

2.4.Cytotoxic activity

The cytotoxicity of 1,2,3-traizole analogs **(7a-x)** were investigated against HeLa, CEM, L1210 and HEK293T cell lines according to the literature (Baraldi et al., **2004,** Sujeet et al., **2014**). The IC_{50} were calculated and expressed in μM (Table 1 and Supplementary fig. 1S). All experiments were performed in triplicate.

Further, the cytotoxic activity of compound **7c** was analyzed using Guava Via Count Reagent (Merck Millipore, Burlington, MA, USA) according to manufacturer's instructions. In brief, after 24 and 48h treatment with **7c**, cells were diluted with the reagent containing 7-AAD and then incubated at room temperature in the dark for 5 minutes. After incubation, cells were analyzed by flow cytometry.

2.5.Analysis of cell death mechanisms

Discrimination between apoptotic and necrotic events was performed by using Guava Nexin Reagent (Merck Millipore). This reagent, containing 7-AAD and annexin V-phycoerythrin (PE), is able to distinguish apoptotic and necrotic events. Cells were exposed to **7c** for 24h and then diluted in Guava Nexin Reagent. After incubation of 20 minutes at room temperature in the dark, cells were analyzed by flow cytometry. Three cell populations can be detected: live cells (annexin− / 7-AAD−), early apoptotic cells (annexin+ / 7-AAD−), and late apoptotic or necrotic cells (annexin+ / 7-AAD+).

To evaluate the induction of non-apoptotic cell death pathways, cell viability was analyzed using SYTOX™ Green Nucleic Acid Stain (Thermo Fisher Scientific), according to manufacturer's protocol. SYTOX™ Green Nucleic Acid Stain is a fluorescent and cell membrane impermeable dye that could easily penetrate only compromised membranes of dead cells, where it binds DNA, thus increasing its fluorescence. Briefly, after pre-treatment of 1h with the different chemical inhibitors and treatment of 24 and 48h with **7c**, cells were supplemented with SYTOX™ Green Nucleic Acid Stain 10nM and after incubation of 20 minutes at room temperature in the dark, cells were analyzed by flow cytometry.

2.6.Measurement of mitochondrial potential

Analysis of mitochondrial membrane potential was assessed using MitoProbeTM DilC1(5) Assay kit (Molecular Probes, Thermo Fisher Scientific), according to manufacturer' instructions. The dye DilC1(5) (1,1′,3,3,3′,3′-hexamethylindo dicarbo-cyanine iodide) accumulates in mitochondria with active membrane potential. The intensity of DilC1(5) staining decreases when cells are treated with agents that disrupt mitochondrial potential. Briefly, after 24h of treatment with **7c**, 10^6 cells were washed and supplemented with 50nM DilC1(5) for 20 minutes at 37°C, 5% CO_2. Then, cells were washed and resuspended in PBS 1X for flow cytometric analysis. CCCP 50μM was used as positive control. Results were expressed as % of cells with decreased mitochondrial potential compared to untreated cells.

2.7.Evaluation of caspase-8 and caspase-3 activity

Caspase activity was assessed using Caspase 8 Colorimetric Protease Assay Kit or Caspase 3 Colorimetric Protease Assay Kit, respectively (both purchased by Thermo Fisher Scientific), according to manufacturer's instructions. Briefly, after 24h treatment, cells were washed in PBS 1X analyzed by adding Cell Lysis Buffer on ice for 10 minutes. Then, cellular lysates were centrifuged and collected, and protein concentration has been normalized according to Bradford assay (Bradford,1976). Cellular lysates wereincubated for 2 h at 37°C in the dark with 2X Reaction Buffer, containing DTT 10mM and caspase-8 or caspase-3

substrate 200μM. Both substrates consist of a synthetic tetrapeptide, IETD (Ile-Glu-Thr-Asp) specific for caspase-8, and DEVD (Asp-Glu-Val-Asp) specific for caspase-3, which are conjugated with the chromophore p-nitroanilide (pNA). When caspases are active, the specific substrate is cleaved from the chromophore and free pNA is used as a reporter, whose absorbance is measured at 405 nm, using the microplate reader Victor X3 (Perkin Elmer). Caspases activity was expressed as the fold increase of treated cells compared to untreated cells.

2.8.Measurement of ROS generation

Intracellular ROS generation was assessed using the probe 2′,7′–dichlorodihydrofluoresceine (H2DCFDA) (Sigma Aldrich). H2DCFDA is a non-fluorescent and cell-permeable probe which is hydrolyzed by intracellular esterases of viable cells into 2′,7′–dichlorohydrofluorescein (H2DCF). In turn, H2DCF is oxidized in presence of ROS into 2′,7′–dichlorofluorescein (DCF), which is highly fluorescent. In brief, 20 minutes before the different time end points (1, 3 or 6h of treatment with**7c**) H2DCFDA 10 μM was added in each well. Then, cells were incubated for 20 minutes at 37 °C and 5% CO_2 and, after incubation, 1×10^6 cells were centrifuged, resuspended in PBS 1X, and analyzed by flow cytometry. Intracellular ROS levels were expressed as fold increase of treated cells compared to untreated cells.

2.9.Cell-cycle and cell-cycle-related proteins expression analysis

After treatment with **7c** for 6 and 24 h, cells were fixed with 70% ice-cold ethanol; after washing, cells were suspended in 200 μL Guava Cell Cycle Reagent (Merck Millipore), containing propidium iodide, and incubated 30 minutes at room temperature in the dark before analysis by flow cytometry. The percentages of cells in G0/G1, S, and G2/M phases were quantified by the analysis of DNA content based on the use of Guava Cell Cycle Reagent.

In order to analyze the expression of cyclin A, cyclin B1 and CDK1, after treatment for 24h, cells were fixed by 70% cold ethanol and permeabilized using 0.25% cold Triton X-100 in Wash Buffer (WB; PBS 1X + 1% bovine serum albumin). Then, samples were washed and incubated with the corresponding primary antibody anti-cyclin A (1:50, Invitrogen, Thermo Fisher Scientific), anti-cyclin B1 (1:50, Invitrogen, Thermo Fisher Scientific), and anti-CDK1 (1:200, Invitrogen, Thermo Fisher Scientific) for 30 minutes. Next, cells were washed in WB and stained with the respective secondary antibody (anti-mouse 1:200; anti-rabbit 1:200; Invitrogen) for other 30 minutes. Cells were washed and then analyzed by flow cytometry, recording the mean fluorescence intensity (MFI) values. Expression of Cyclin A, Cyclin B1, and CDK1 were indicated as fold increase of treated cells compared to untreated cells.

2.10. Analysis of DNA damage

The genotoxic potential of **7c** was assessed evaluating the phosphorylation of histone γ-H2A.X, as marker of DNA double strand breaks. Briefly, after treatment of 5h with increasing concentrations of **7c**, cells were fixed, permeabilized and incubated for 30 minutes in the dark at room temperature with an anti γ-H2A.X-Alexa Fluor® antibody (Merck Millipore, Darmstadt, Germany). Then, samples were analyzed via flow cytometry. Phosphorylation of histone γ-H2A.X was expressed as fold increase of treated cells compared to untreated cells. Etoposide 10μg/mL was used as positive control.

2.11. Flow cytometry

All flow cytometric analyses were performed using an EasyCyte 5HT flow cytometer (Guava Technologies-Millipore, Hayward, CA, USA).

2.12. ADME evaluation

The 3D (three dimensional) structures of the molecules were drawn using Avogadro v1.2.0 (Hanwell et al., 2012) and the structures were optimized using MMFF94s force field. SwissADME webserver (Daina et al., 2014, 2017) were used to evaluate ADME parameters, pharmacokinetics and drug-like nature of the molecules.

2.13. Molecular docking simulations

In docking simulations, the X-ray crystal structure (Pdb ID: 6P8Q) of EGFR was used as target. The co-ligand of this structure is 10-benzyl-2-fluoro-5,10-dihydro-11*H*-dibenzo[*b*,*e*][1,4]diazepin-11-one. In addition, we performed all theoretical calculations for the co-ligand and melphalan, reference drug, in order to compare with the results obtained for the synthesized compounds. For docking simulations, all ligands and target were prepared by using PyRx software (Dallakyanand Olson, 2015) and subsequently the docking experiments were performed using theAutoDockVina software (Trott and Olson, 2010) with Lamarckian genetic algorithm (LGA) (Solis and Wets, 1981, Huey et al., 2007). The visualizations of docking simulations results were conducted using Discovery studio (Biovia2017).

Statistical analysis

All experiments are expressed as the mean ± SEM of at least three independent experiments. Statistical analyses were performed by Repeated Measures ANOVA; Tukey or Dunnett or Bonferroni were used as a post-test, using the statistical software GraphPad InStat 6.0 version(GraphPad Prism, San Diego, CA, USA). p-values below 0.05 were considered as significant and represented as * $p < 0.05$, ** $p < 0.01$, *** $p < 0.001$, and **** $p < 0.0001$.

3. Results and discussion

3.1.Chemistry

A series of twenty-four1,2,3-triazole derivatives (**7a-x)**wasprepared following **Scheme 1**.4-(Prop-2-ynyloxy)-benzaldehyde**(3)**was synthesized by reacting 4-hydroxybenzaldehyde (**1)**with propargyl bromide (**2)**in presence of potassium carbonate (K_2CO_3) and dry dimethylformamide (DMF), then was treated with benzyl azides(**4A-D)** in presence of sodium ascorbate and copper sulphate pentahydrate ($CuSO_4{\cdot}5H_2O$) to get 4-((1-benzyl-1*H*-1,2,3-triazol-4-yl)methoxy)benzaldehydes**(5A-D)** in good yield. Finally, the (Z)-3-(4-((1-benzyl-1*H*-1,2,3-triazol-4-*yl*)methoxy)benzylidene)indolin-2-ones (**7a-x)** were obtained byrefluxing triazole-aldehydes **(5A-D)**and indolin-2-one (**6E-J)**in methanol with piperidine.

The feasibility and mechanism of indolin-2-one (**6E-J**) reaction with 4-((1-arylmethyl-1*H*-1,2,3-triazol-4-yl)methoxy)benzaldehydes (**5A-D**) catalysed by piperidine follows Knoevenagel condensation (Figure 2). An enol intermediate is formed initially between indolin-2-one **(6E-J)** and piperidine. This enol reacts with 4-((1-arylmethyl-1-1,2,3-triazol-4-yl)methoxy)benzaldehydes (**5A-D**) and the resulting aldol undergoes subsequent base-

induced elimination to form the 3-(4-((1-benzyl-1*H*-1,2,3-triazol-4-yl)methoxy benzylidene)indolin-2-ones (**7a-x**).

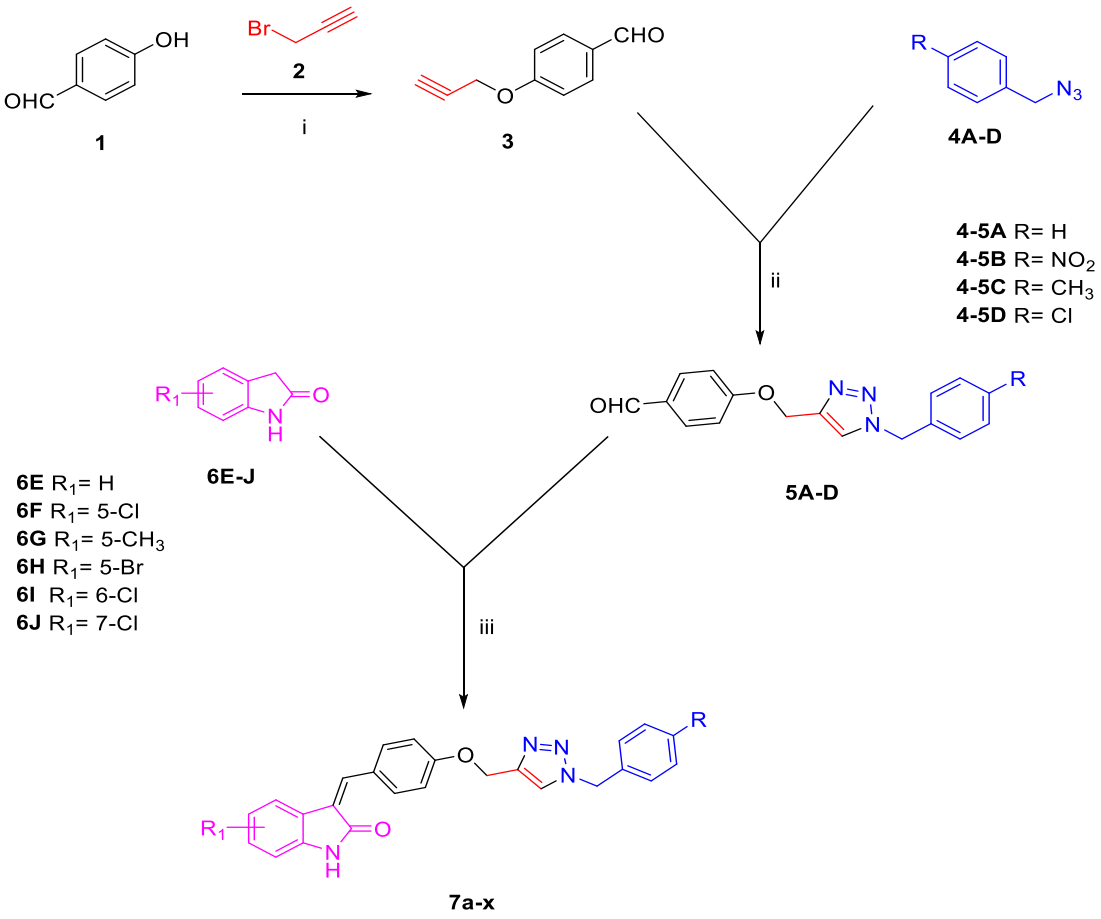

Reagents and conditions: i) K_2CO_3, DMF, 25°C, 10 h
ii) $CuSO_4.5H_2O$, Sodium ascorbate, t-butanol,35°C, 5 h
iii) piperidine, methanol, reflux

Comp	R	R_1	Comp	R	R_1
7a	H	H	**7m**	CH_3	H
7b	H	5-Cl	**7n**	CH_3	6-Cl
7c	H	5-CH_3	**7o**	CH_3	5-CH_3
7d	H	5-Br	**7p**	CH_3	5-Br
7e	H	7-Cl	**7q**	CH_3	5-Cl
7f	H	6-Cl	**7r**	CH_3	7-Cl
7g	NO_2	5-Cl	**7s**	Cl	H
7h	NO_2	5-Br	**7t**	Cl	5-Cl
7i	NO_2	6-Cl	**7u**	Cl	5-Br
7j	NO_2	7-Cl	**7v**	Cl	5-CH_3
7k	NO_2	H	**7w**	Cl	6-Cl
7l	NO_2	5-CH_3	**7x**	Cl	7-Cl

Scheme 1. Synthesis of compounds **7a-x.**

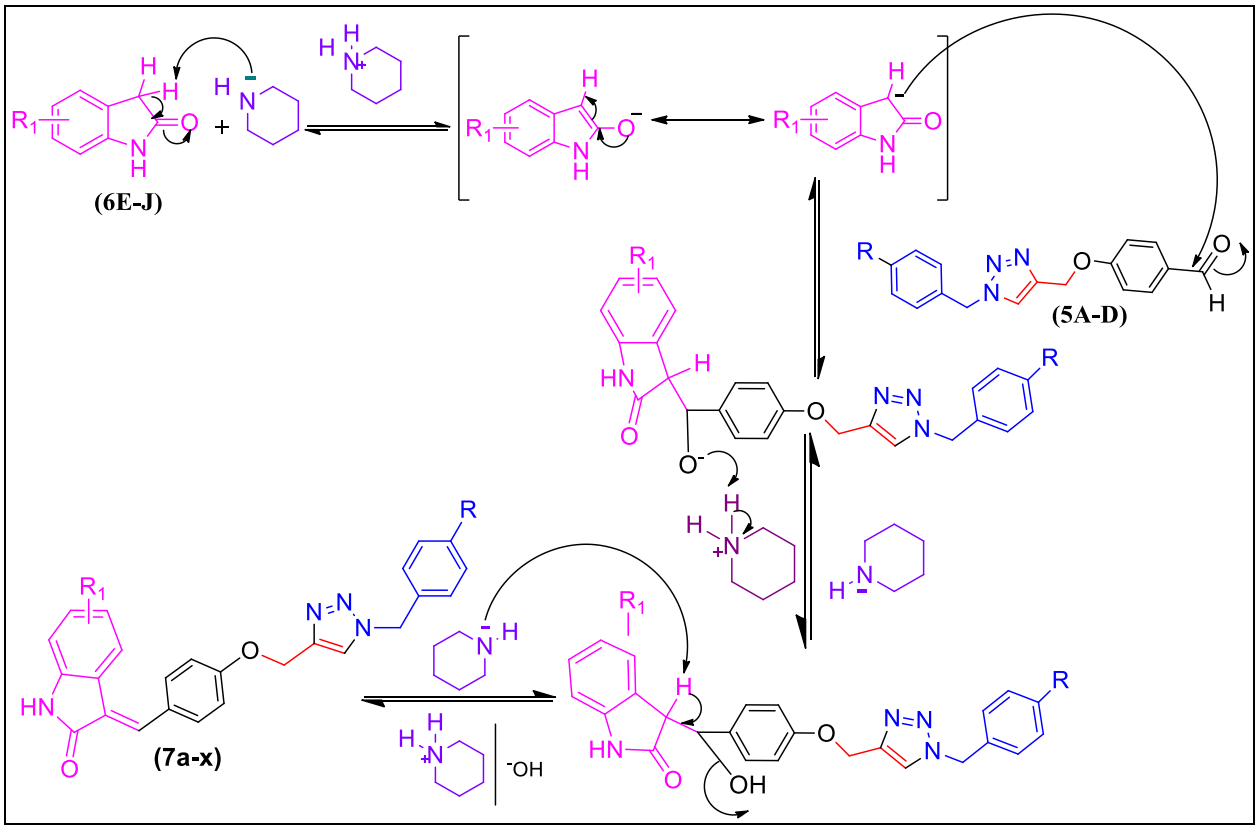

Figure 2. Mechanism involved in the synthesis of indolin-2-one linked 1,2,3-triazole derivatives(**7a-x**).

All newly synthesized triazoles **(7a-x)** were characterized by their Fourier transform infrared (FTIR) and proton/carbon nuclear magnetic resonance(^{1}H/^{13}C-NMR)spectral data. The FTIR spectra of **7a-x**showed stretching absorption bands between 3247-3141 (N-H), 3090-3010(C-H, ar.), 2950-2798 (C-H, ali.), 1701-1672 (>C=O), 1623-1582 (>C=N-), 1554-1449 (>C=C<) and 1226-1167 (-O-) cm^{-1}. Absorption bands for -CH_2- bending were observed in the range of 1489-1448 cm^{-1}.Compound **7c**, **7l-r** and **7v**showed -CH_3 bending absorption bands appearing at 1389-1376 cm^{-1}. Absorption bands for -NO_2 stretching in **7g-l** were observed in the range of 1594-1514 cm^{-1}. In ^{1}H-NMR spectra, the -NH proton as singlet was observed between δ 11.04-10.41 ppm whereas, triazole ring proton appeared in the range of δ 8.41-8.27 ppm. Prominent signals between δ 8.50-5.90 ppm represent aromatic protons and, signal between δ 7.92-7.51 ppm appeared for benzylidene -CH. Presence of -CH_2- groups was confirmed by a singlet signal between δ 5.81-5.50 (-OCH_2-) and δ 5.29-5.22 (-NCH_2-) ppm. Methyl protons of **7c, 7l-r** and **7v** were seen in the range of δ 2.67-2.17 ppm.The ^{13}C NMR spectra displayed peaks between δ 169-166 ppm for C=O of 2-oxindole, peaks between δ 159-108 ppm for aromatic carbons, peaks at δ 61 ppm for –OCH_2-, peaks between δ 51-53 ppm for triazole –NCH_2- and at δ 20-21 ppm for methyl carbon.

3.2.Invitro cytotoxicity evaluation

All 1,2,3-triazole analogs(**7a-x**) were preliminary screened against murine L1210 leukemia cells, human CEM T-lymphocytic and cervix carcinoma HeLa cells. The results are presented in **Table 1**. Compounds were evaluated in the HeLa and CEM bioassays to ascertain if these triazoles (**7a-x**) are toxic to human cells or not. A number of drugs used in the cancer chemotherapy are toxic to murine leukemia L1210 cells and that made us to use L1210 cell line. The alkylating agent melphalan was used as positive control. In CEM screens, most of the compounds exhibited a good cytotoxic activity either in presence or absence of substituents on 2-oxindole and benzyl group of triazole. Among the tested compounds, **7c** and **7w** proved to be as potent as melphalan, whereas only three compounds **7b, 7j** and **7n** exhibited poor activity in comparison to melphalan. In HeLa screen, the compounds **7a, 7c, 7m, 7o, 7s, 7v** and **7w** showed good cytotoxicity, whereas **7g, 7h, 7j-l, 7t, 7u** and **7x** showed moderate cytotoxic activity. In case of murine leukemia L1210, most of the compounds exhibited moderate to poor cytotoxicity except **7c, 7o** and **7v**. Moreover, the most potent cytotoxic compound **7c** was further analyzed in order to evaluate its mechanism of action and studied for drug likeliness by using SwissADME webserver.

3.3.Structure activity relationships

Compounds **7** were less effective against murine L1210 leukemia cells in comparison to standard melphalan (2.13 µM). However, the introduction of a methyl group at position 5 of indolin-2-one, led to the most effective compounds, namely **7c**, **7o** and **7v**, with IC_{50} 3.0, 5.3 and 4.8 µM respectively, against murine L1210 cells. Substituents different from the methyl group on indolin-2-one and benzyl group did not improve cytotoxicity against murine L1210 leukemia cells. Substitutions made at position 5, 6 or 7 on indolin-2-one and at position 4 on benzyl group increased (compounds **7c**, **7w**) or maintained the cytotoxic activity against CEM cells, except for compounds **7b**, **7f**, **7j** and **7r**. In general, replacement of hydrogen with $-CH_3$, -Cl or $-NO_2$ at position 4 of benzyl group, as well as substitution at position 5, 6 or 7 on indolin-2-one, improved cytotoxicity against HeLa cells.

Table 1.*Invitro* cytotoxicity data of synthesized indolin-2-one linked 1,2,3-triazole analogs(**7a-x**).

Compound	**IC_{50} (µM)**		
	L1210	**CEM**	**HeLa**
7a	8.1 ± 2.2	3.6 ± 2.5	4.6 ± 0.0
7b	>250	33 ± 3.4	133 ± 18
7c	3.0 ± 0.9	1.5 ± 0.6	3.4 ± 0.6
7d	150 ± 14	6.7 ± 1.9	36 ± 0.6
7e	29 ± 1.0	7.3 ± 1.9	38 ± 3
7f	44 ± 4.0	18 ± 4.0	66 ± 3.4
7g	32 ± 1.0	5.0 ± 0.7	7.8 ± 2.9
7h	32 ± 1.5	6.0 ± 1.1	9.2 ± 1.7
7i	19 ± 2.0	11 ± 6.0	20 ± 1.0
7j	17 ± 9.0	67 ± 2.5	7.1 ± 4.4
7k	34 ± 2.0	3.9 ± 0.8	11 ± 3.0
7l	30 ± 4.0	4.6 ± 0.4	12 ± 3.0
7m	19 ± 4.0	4.4 ± 0.6	4.8 ± 0.1
7n	31 ± 4.0	33 ± 3.0	70 ± 3.5
7o	5.3 ± 0.5	3.8 ± 0.8	4.4 ± 0.6
7p	38 ± 2.5	7.4 ± 1.7	16 ± 1.0
7q	24 ± 6	5.7 ± 1.0	15 ± 1.0
7r	100 ± 13	18 ± 17	31 ± 3.9
7s	12 ± 0.9	3.8 ± 1.7	3.7 ± 0.1
7t	20 ± 4.0	5.3 ± 1.4	13 ± 1.0
7u	20 ± 6.0	5.5 ± 0.1	12 ± 6.0
7v	4.8 ± 1.1	4.0 ± 0.6	3.7 ± 0.4
7w	14 ± 1.1	1.7 ± 0.8	3.9 ± 0.4
7x	17 ± 3.0	6.8 ± 0.7	8.1 ± 1.9
Melphalan	2.13±0.02	1.4±0.4	NT

NT= Not tested.

3.4.Compound 7c exclusively induces caspase-dependent apoptosis in Jurkat cells and activates both intrinsic and extrinsic apoptotic pathways

We next investigated the molecular mechanisms involved in **7c's** cytotoxicity by flow cytometry. The screening of the newly synthesized 1,2,3-triazole analogs unveiled that the most potent compound**7c** was highly cytotoxic onCEMleukemiacells. Therefore,we preliminary tested **7c** on different leukemia cell lines (*i.e.* HL-60, CEM, and Jurkat) using a cytofluorimetric technique, as described in materials and methods. Among all, Jurkat cells were found to be the most sensitive to **7c** cytotoxicity (data not shown) and thus were chosen to deeper investigate the anticancer potential of compound **7c**.

Different cell-death modalities were defined based on morphological alterations associated with specific mechanisms whereby dead cells are eliminated. These modalities include three types of cell demise: type I or apoptosis, type II or autophagy and type III or necrosis. Of note, apoptosis and autophagy are both forms of programmed cell death (PCD), or canonical cell death, while necrosis was for a long time considered as a non-physiological process (*i.e.*non-PCD) that occurs as a result of infection or injury (Galluzzi et al., 2018). Among all types of PCDs, apoptosis is definitely the most studied and known mechanism of cell demise. Apoptosis is mainly mediated by two pathways: the extrinsic, or death receptor pathway, and the intrinsic, or mitochondrial pathway. The extrinsic apoptotic pathway is triggered by extracellular ligands that bind to specific transmembrane death receptors (DRs), leading to the activation of pro-caspase-8/-10. Once activation of caspase-8/-10 occurs, they cleave and activate effector caspase-3/-7, driving to apoptosis execution (Galluzzi et al., 2018). The intrinsic or mitochondrial apoptotic pathway, instead, is triggered by a wide variety of extracellular and intracellular stress stimuli that lead to the irreversible and diffuse mitochondrial outer membrane permeabilization (MOMP) (Galluzzi et al., 2018). Once the mitochondrial permeability is destroyed, the transmembrane potential collapsesand multiple apoptogenic factors, as cytochrome c, are released into the cytoplasm (D'Arcy et al., 2019).Active caspase-9 catalyzes the proteolytic activation of executioner caspase-3 and -7, leading to apoptotic cell death (D'Arcy et al.,2019).

In order to analyze if **7c** triggers apoptotic or necrotic cell death,we performed the annexin V/7-AAD assay. The use of annexin V binding to phosphatidylserine *plus* 7-amino-actinomycin D (7-AAD) allows detecting apoptotic cells (annexin V^+/7-AAD^- cells) and necrotic cells (annexin V^+/ 7-AAD^+ cells) (Zimmermann et al., 2011).After 24h of treatment, **7c** increased the fraction of apoptotic cells in a dose-dependent manner. The percentage of apoptotic cells started to increase from the concentration 2μM (14% *versus* 3.9% in untreated cells), and further increased up to the highest tested concentration, where they reached about 27%. Alongside the increase in apoptotic cells, the percentage of necrotic cells remained constant between 3% and 7% at all tested concentrations (Figure 3).

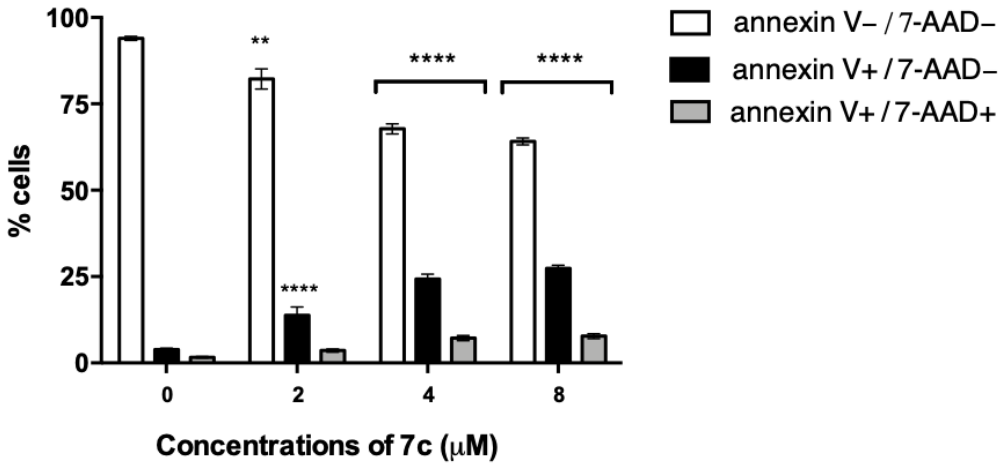

Figure 3. Percentage (%) of viable (annexin V^-/7-AAD^-), early apoptotic (annexin V^+/7-AAD^-), and late apoptotic or necrotic (annexin V^+/ 7-AAD^+) cells after 24h treatment of Jurkat cells with increasing concentrations of **7c**. ** p< 0.01; **** p< 0.0001 *versus* untreated cells.

At this point, some of the molecular pathways modulated by the newly synthesizedcompound**7c** have been explored. Caspase-3 is an effector caspase activated from both the intrinsic and extrinsic apoptotic pathway (Nagata et al., 2018). Its activity was markedly increased after treatment with **7c**, up to about 8 times at concentrations 4 and 8μM (Figure 4), confirming apoptosis induction by the indole-based derivative. Next, to investigate the involvement of the extrinsic apoptotic pathway in the pro-apoptotic activity of **7c**, we analyzed the activity of caspase-8. Its activity increased up to about 4 times at concentrations 4 and 8μM after **7c** treatment (Figure 4).To assess the involvement of the intrinsic apoptotic pathway, we measured the decrease in mitochondrial transmembrane potential. A significant increase in cells with reduced potential was recorded starting from concentration 4μM (35% of cells with decreased potential *versus* 7.4% in untreated cells) and the percentage further increased to about 46% at 8μM (Figure 4).On the whole, our results indicate that **7c** activates both apoptotic pathways.

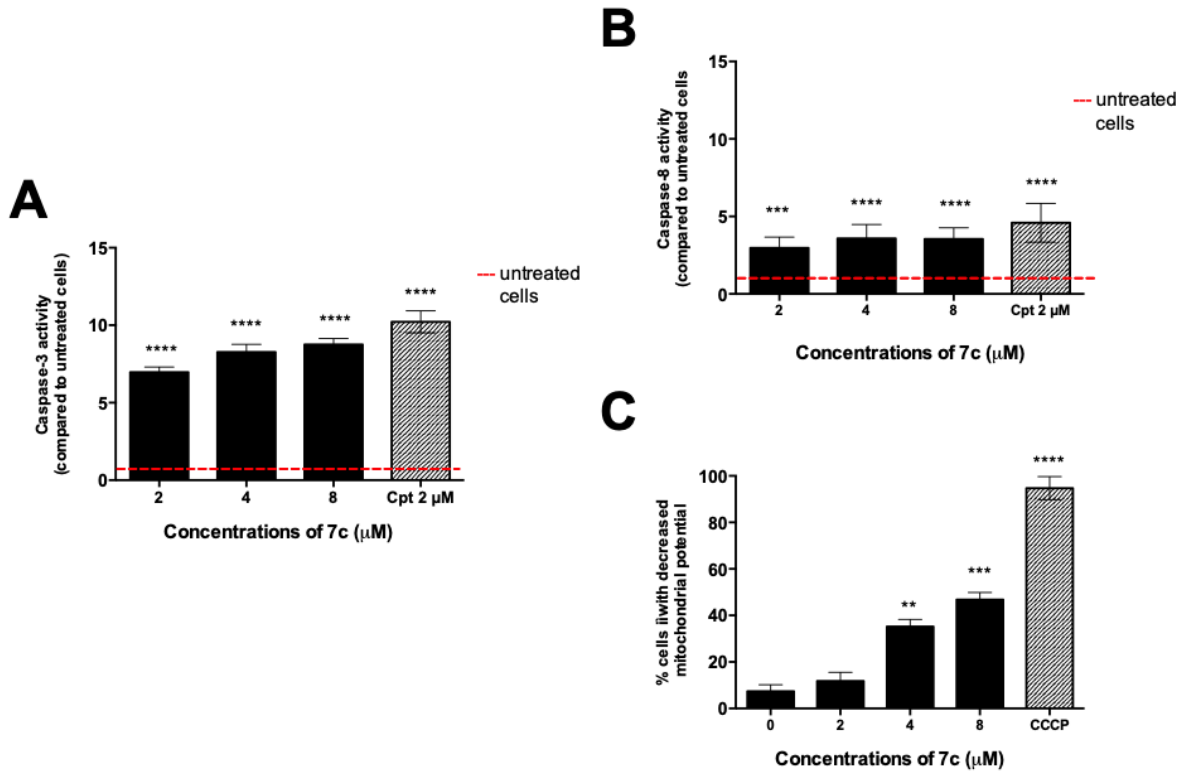

Figure 4. Activity of caspase-3 (A) and caspase-8 (B) and percentage (%) of cells with decreased mitochondrial potential (C) after 24h treatment of Jurkat cells with increasing concentrations of **7c**. Cpt (camptothecin) and CCCP (carbonyl cyanide 3-chlorophenylhydrazone) were used as positive controls. **p< 0.01; ***p< 0.001; ****p< 0.0001 *versus* untreated cells.

The ability of **7c** to activate both apoptotic pathways is noteworthy. Indeed, cancer cells are characterized by high genetic and genomic instability, which can lead to the mutation of some of the molecular actors involved in a specific apoptotic pathway. As an example, overexpression of Bcl-2 (B-cell lymphoma 2) and associated anti-apoptotic proteins, impaired assembly of a functional apoptosome, inactivation of caspase-8, decreased expression or gene mutations of Fas (Mohammad et al., 2015, Fulda, 2009) (Fas cell surface death receptor, also called CD95) are just some of the multiple mechanisms involved in apoptosis resistance. The result is the development of drug resistance and the lack of efficacy of anticancer therapy (Mohammad et al., 2015).Thus, evidence that compound **7c** is able to modulate both apoptotic pathways could potentially increase its clinical potential.

In recent years, accumulating evidence increasingly pointed out that various non-apoptotic forms of PCD can be triggered independently of apoptosis or when the apoptotic process appears to be altered or inhibited. Non-apoptotic cell death pathways differ from the apoptotic process not only in morphological terms, but also in biochemical terms and include various PCD pathways (Tait et al., 2014), such as ferroptosis, necroptosis and parthanatos. Necroptosis is a highly regulated cell death mechanism, which shares the typical morphological features of necrosis. The process of necroptosis is controlled in an apoptosis-deficient environment by receptor interacting protein RIP1 and RIP3. Together with RIP1 and 3, mixed lineage kinase domain like pseudokinase (MLKL) is also involved in necroptosis (Qin et al., 2019). Indeed, after its phosphorylation by active phosphorylated RIP3, MLKL oligomerizes and translocates to plasma membrane, which is a crucial event for

necroptosis execution (Chen et al.,2019). On the other hand, ferroptosis is a non-apoptotic form of cell death that can be triggered by small molecules or conditions that inhibit glutathione biosynthesis or the glutathione-dependent antioxidant enzyme GPX4 (glutathione peroxidase 4). This lethal process is defined by the iron-dependent accumulation of lipid reactive oxygen species (ROS), which leads to cell demise (Cao et al.,2016). Finally, parthanatos is a peculiar form of non-canonical PCD characterized by plasma membrane rupture without the formation of apoptotic bodies and DNA fragments. Biochemically, parthanatos is a PARP-1-dependent PCD pathway, as it is mediated by the hyperactivation of PARP-1, due to a DNA-basemodification (Galluzzi et al., 2018).

Hence, to determine whether **7c** could activate non-canonical cell death programs, Jurkat cells were pre-treated for 1h with different chemical inhibitors[*i.e.* Z-VAD-FMK, olaparib, necrostatin-1s, ferrostatin-1, deferoxamine mesylate (DFO), and vitamin E] in order to inhibit apoptosis, parthanatos, necroptosis and ferroptosis, respectively. Then, after pre-treatment, cells were treated with **7c**8µM for 24h and 48h and cell viability was analyzed by flow cytometry.

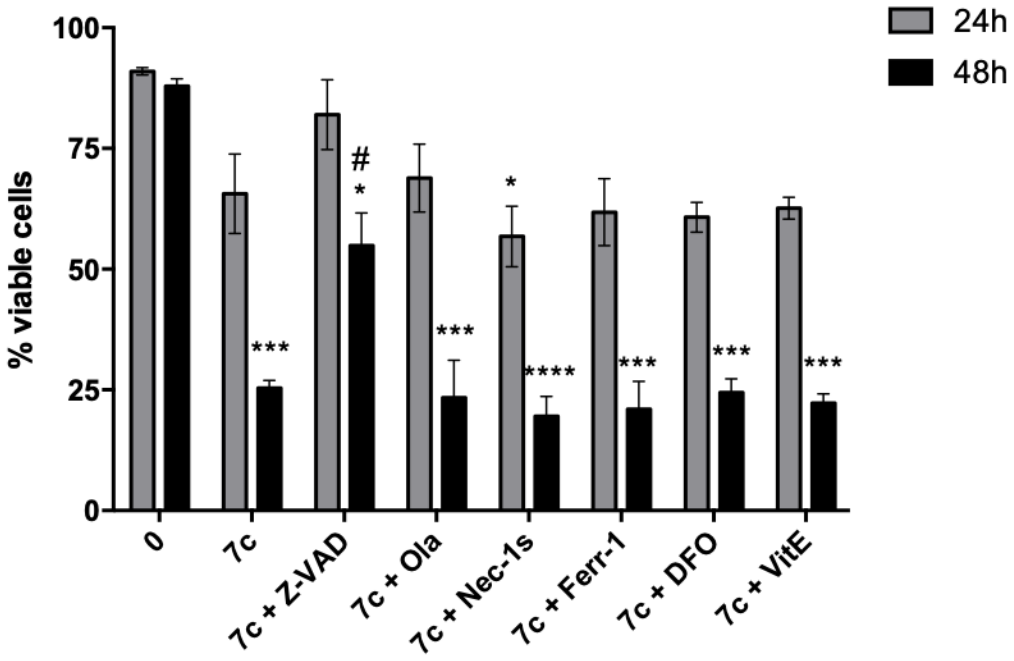

Figure 5. Percentage (%) of viable cells after pre-treatment for 1h with Z-VAD-FMK (Z-VAD), olaparib (Ola), necrostatin-1s (Nec-1s), ferrostatin-1 (Ferr-1), DFO, or vitamin E (VitE) following 24h and 48h treatment with **7c** 8µM. *p< 0.05; ***p< 0.001; ****p< 0.0001 *versus* untreated cells. # p< 0.05 *versus* **7c**-treated cells.

Among all the pharmacological inhibitors, only the pan-caspase inhibitor Z-VAD-FMK increased Jurkat cells viability, just partially after 24h and significantly after 48h (**Figure 5**). Recorded cell viability of Z-VAD-FMK pre-treated cells was 82% at 24h (*versus* 65% of **7c**-treated cells) and 55% at 48h (*versus* 25% of **7c**-treated cells). Our results indicate that**7c** does not induce non-canonical cell death as ferroptosis, necroptosis or parthanatos, but exclusively caspase-dependent apoptosis.

Regarding the ability of indoles and indole derivatives, no evidence has been found about their ability to trigger non-canonical cell death. A study conducted by Behnisch-Cornwell and colleagues, for example, investigated ferroptosis induction in human cervical

cancer SISO cells by a series of newly synthesized indole-based pentathiepins, establishing that these new derivatives induce apoptosis rather than ferroptosis (Behnisch-Cornwell et al., 2020).

3.5.ROS are not involved in the pro-apoptotic activity of 7c

ROS play a central role in cell signaling and represent one of many stimuli that leads to apoptotic cell death(Galluzzi et al., 2018).We measured intracellular ROS levels after different treatment times with **7c**. **7c**did not induce any significant modulation of ROS levels (Figure 6), thus indicating that ROS generation is not involved in the orchestration of the cytotoxic response evoked by the newly triazole derivative **7c**.

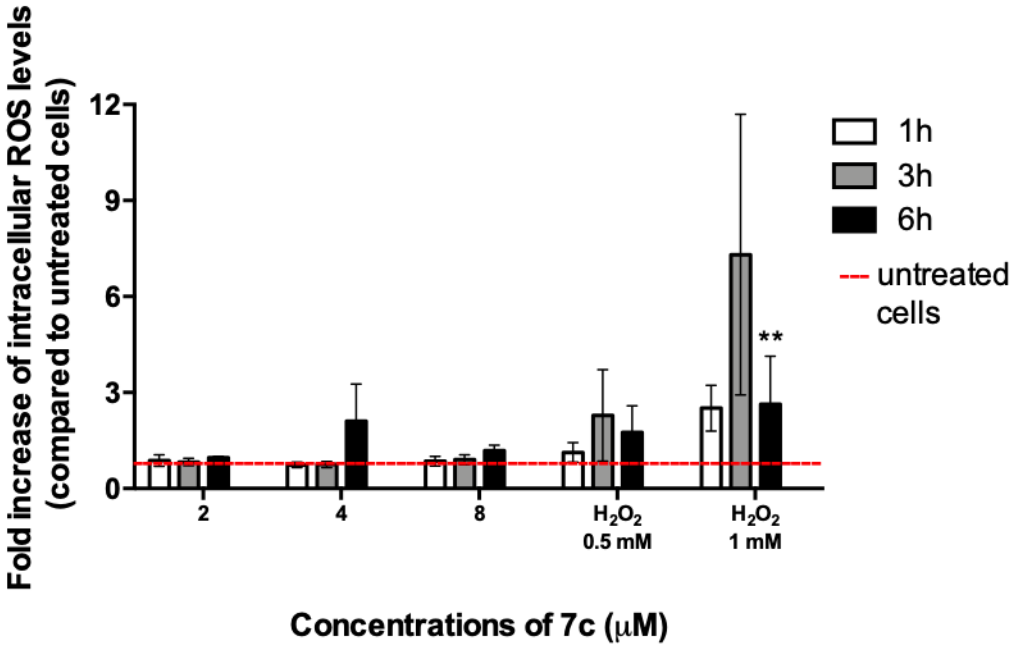

Figure 6. Intracellular ROS levels, expressed as fold increase *versus* untreated cells, of Jurkat cells treated with increasing concentrations of **7c** for different time points. H_2O_2 0.5 and 1mM were used as positive control. **p< 0.01*versus* untreated cells.

*3.6.Compound **7c** causes cell-cycle perturbations*

Cell cycle is a sequence of closely coordinated molecular processes that control DNA replication and chromosome division, ultimately leading to cell division and transfer of genetic material. Cell cycle resides into four distinct phases: G1 (gap), S (synthesis), G2 (gap) and M (mitosis), all strictly controlled by cyclins and cyclin-dependent kinases (CDKs) (Hochegger et al., 2008). Since the G1/S and G2/M checkpoints finely control cell proliferation, cell-cycle arrest is considered one of the most common events triggering the inhibition of cell proliferation. Hence, to explore the cytostatic potential of **7c** we analyzed cell-cycle progression of **7c**-treated cells together with the expression of some cyclins and CDKs. The treatment with increasing concentrations of **7c** induced a significant accumulation of cells in the G2/M phase. Starting from the concentration 4μM the accumulation of cells in the G2/M phase appeared to be statistically significant, with 57% *versus* 31% of untreated cells; at the highest tested concentration, the percentage further increased up to 64%. This observed increase was accompanied, at all tested concentrations, by a slight compensatory decrease in cells in the G0/G1 phase, from 59% of untreated cells to 23% of cells treated with **7c**8μM (Figure 7).

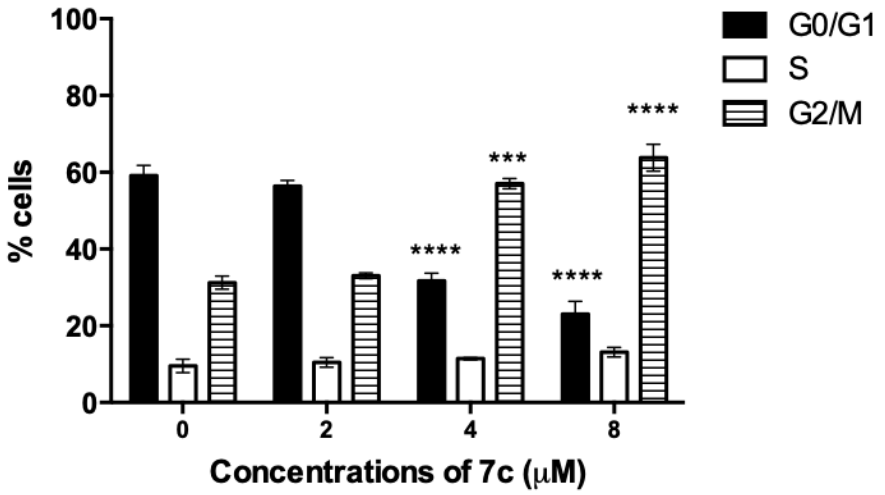

Figure 7 Cell-cycle distribution after Jurkat treatment with **7c** for 24h. ***p< 0.001; ****p< 0.0001 *versus* untreated cells.

As mentioned before, cell cycle is tightly controlled by CDKs and cyclins. Briefly, in the G1 phase, activation of cyclin D-CDK4/6 complex leads to the phosphorylation of RB1 protein, thus promoting the expression of different genes that regulate cell-cycle progression. Then, when cells progress into the S phase, cyclin A starts to be synthesized, thus replacing cyclin D and reaching its maximal expression in the G2 phase until its degradation during the transition from the G2 to the M phase of cell cycle. Cyclin B, instead, starts to be expressed from the G2 phase and extensively accumulates prior to mitosis. Finally, CDK1 could be activated by both interphase cyclins (*i.e.*cyclins D, E, and A) and mitotic cyclin B (Hochegger et al., 2008).Toexplorewhether**7c**-treated cells accumulate in G2 or M phase, the expression of cyclin A and B1, and CDK1 was analyzed. After 24h of treatment, **7c** did not modulate the expression of cyclin B1 and CDK1; however, a slight downregulation of cyclin A was observed (Figure 8). As we noticed a decrease in cyclin A expression, but not a modulation of cyclin B and CDK1, we could speculate that compound **7c** may block cell-cycle progression during the transition from the G2 to the M phase, where cyclin A starts to be degraded prior to the entry of cells in mitosis. Moreover, this hypothesis could explain why we did not observe any modulation of cyclin B1 and CDK1 expression.

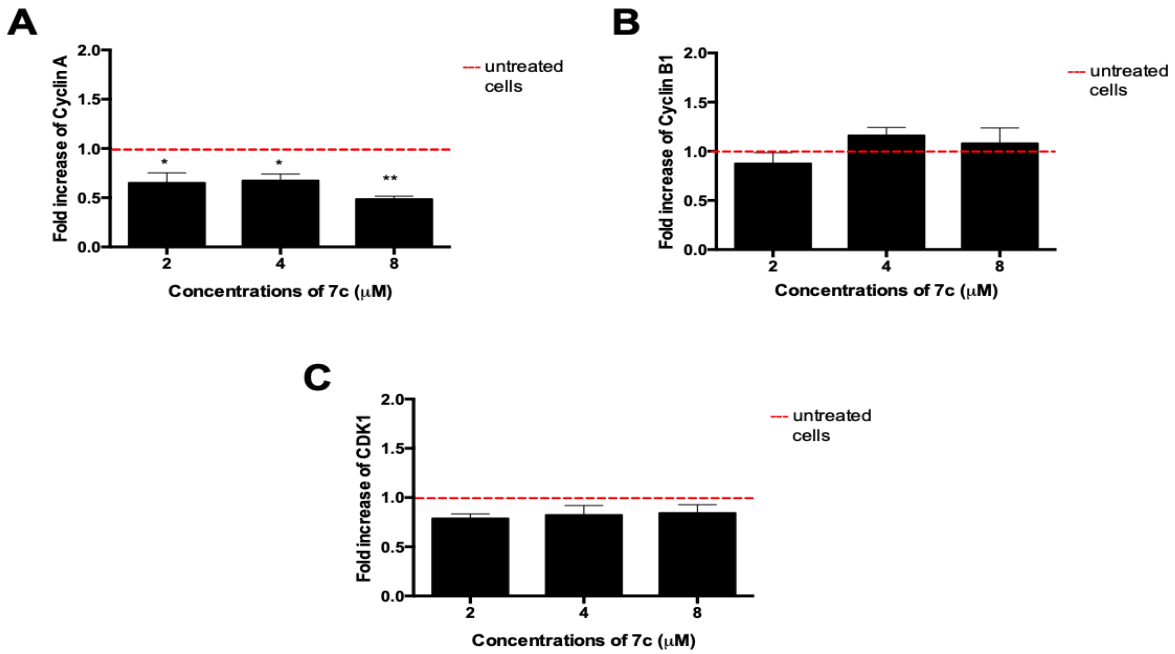

Figure 8. Expression of cyclin A (A), cyclin B1 (B), and CDK1 (C), indicated as fold increase *versus* untreated cells, following 24h treatment of Jurkat cells with increasing concentration of **7c**. *p< 0.05; **p< 0.01 *versus* untreated cells.

*3.7.The pro-apoptotic activity of **7c** is linked to its cytostatic activity*

Next, the pro-apoptotic and cytostatic activities of **7c** were analyzed after 6h of treatment with **7c** to assess whether the two events were related or independent from each other. At 6h of treatment,**7c** did not induce cell death, while a substantial block of cell cycle was already evident (Figure 9). Thus, we can hypothesize that **7c**-induced apoptosis could be a secondary effect, related to its cytostatic activity rather than an independent event.

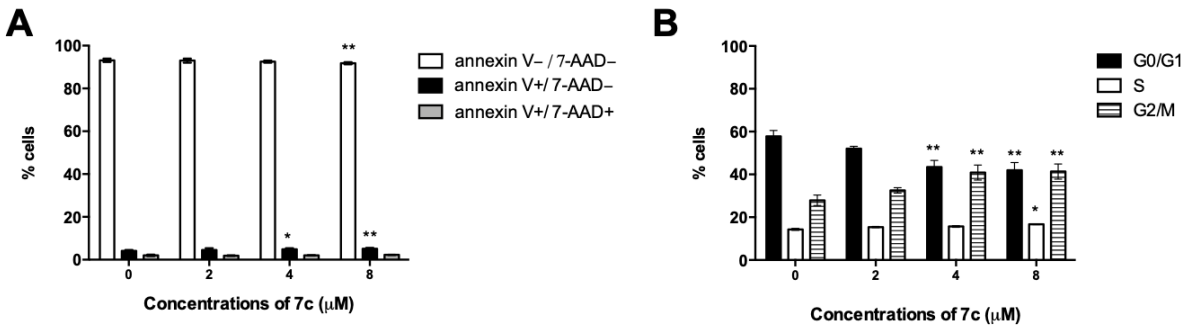

Figure 9. Percentage (%) of viable (annexin V^-/7-AAD^-), early apoptotic (annexin V^+/7-AAD^-), and late apoptotic or necrotic (annexin V^+/ 7-AAD^+) cells (A) and cell- cycle distribution (B) following 6h treatment of Jurkat cells with increasing concentrations of **7c**. *p< 0-05; **p< 0.01 *versus* untreated cells.

*3.8.Compound **7c** lacks genotoxic activity*

Given the interesting anticancer activities observed for **7c**, a preliminary assessment of its toxicological profile was performed by analyzing its genotoxicity. The ability of a compound to cause DNA damage is a crucial factor in determining its toxicological profile, as DNA mutations are involved in the pathogenesis of several degenerative diseases, as cancer (Nohmi, 2018). Additionally, genotoxicity is a dose-independent event, which means that a range of concentrations where genotoxicity does not occur cannot be always established (Giulia et al., 2021). The eventual genotoxic activity of **7c** was verified by analyzing the phosphorylation of H2A.X (P-H2A.X) at Serine 139. P-H2A.X is considered an early cellular response to DNA double-strand breaks; hence, the analysis of this event is useful to detect the ability of a compound to induce DNA damage (Mah et al.,2010). Following 5h treatment of Jurkat cells with **7c**, no significant increase in H2A.X phosphorylation was observed at any tested concentration (Figure 10). Our results are in contrast with what has been observed for other indole derivatives. Indeed, a series of indole hydrazide (Kilic-Kurt et al.,2020)and bis-indolinone derivatives (Amato et al., 2014) induced DNA damage in breast adenocarcinoma MCF-7 cells and in human transformed fibroblasts (BJ-EHLT), as shown by a significant increase in H2AX phosphorylation (Kilic-Kurt et al.,2020,Amato et al., 2014).

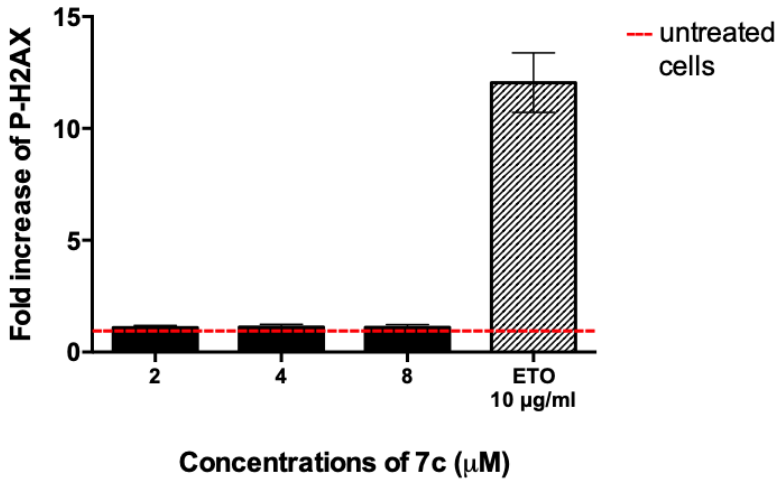

Figure 10. Relative expression of P-H2AX following 5h treatment of Jurkat cells with increasing concentrations of **7c**. Etoposide (ETO) 10µg/mL was used as positive control. **p< 0.01 *versus* untreated cells.

3.9.Effect of 7c in normal cells

To investigate the effect of **7c** on cancer cells compared to normal, it treated 293T cells by 0.5 mM of **7c** and performed a dead test using ethidium bromide stain over a period of 48 hours. The results showed that **7c** was more cytotoxic against L1210 (3 µM), CEM (1.5 µM) and HeLa (3.4 µM) compared to 293T normal cells (7.5 µM) (**Suppl. Fig. 1S**). This suggests that **7c** can effectively kill cells with a high rate of growth which is a hallmark of cancer cells.

3.10. Physicochemical properties and ADME parameters

The physicochemical properties, ADME parameters and the violations of drug-likeness rules of synthesized compounds were listed in **Table 2**. In here, the evaluated physicochemical properties are: the molecular weight (MW), topological polar surface area (tPSA), Molar Refractivity (MR), fraction of sp^3 carbon atoms (Fsp^3) and some Hydrogen Bond properties. tPSA is defined as the sum of surface areas of polar atoms in a molecule and

is used to estimate drug transport properties. Low tPSA values in molecules correspond to a higher propensity for transport and tPSA values obtained for all compounds are within the range of values recommended by various drug-likeness filters. Fsp^3 is a newer parameter (Lovering et al., 2009) used to evaluate drug-likeness properties of molecules. As reported in Table 2, Fsp3 values of all compounds are lower than co-ligand and melphalan. MR is defined as a measure the overall polarity of a molecule and is expected to be in the range from 40 to 130. According to Table 2, MR values for all compounds are within this range. On the other hand, lipophilicity is a valuable parameter that affects drug activity in the human body. LogP values are the most widely used measure of lipophilicity and representsan indicator of drugs permeability to reach the target tissue in the body. The LogP values used by the different drug-likeness filters (MLogP for Lipinski filter (Lipinski et al.,1997), WLogP for Ghose (Ghose et al., 1999) and Egan filters (Egan et al., 2000), XLogP for Muegge filter (Muegge et al., 2001) and their mean values (consensus LogP) were shown in the table 2. The obtained LogP values vary a lot depending on the method used for the prediction and the acceptability limits of the LogP values differ according to drug filters approaches.In this context, when the LogP values are examined in the Table 2, it is observed that the compounds **7t** (XLogP=5.01), **7u** (XLogP=5.08), **7w** (XLogP=5.01) and **7x** (XLogP=5.01) slightly exceed the acceptability limit (XLogP< 5) determined by the Muegge filter. On the other hand, it can be said that all other LogP values meet general standards. ESOL is aqueous solubility parameter of molecules proposed by Delaney (Delaney, 2004) and is considered one of the key physical properties in drug discovery. We observed that ESOL values of all synthesized compound belong to moderately water-soluble class.

On the other hand, there are a lot of filter approach in the literature that suggest a set of rules to evaluate drug-likeness profiles ofmolecules. The filters discussed in this paper and their rules are as follows.

- Lipinski (Pfizer) filter (Lipinski et al.,1997): MW≤500; MLogP ≤4.15; HBA≤10; HBD≤5
- Ghose filter (Ghose et al., 1999): 160≤MW≤480; -0.4≤WLogP ≤ 5.6; 40≤MR≤130; 20≤atoms≤70
- Egan (Pharmacia) filter(Egan et al., 2000): WLogP≤5.88; tPSA≤131.6
- Muegge (Bayer) filter (Muegge et al., 2001): 200≤MW≤600, -2≤XLogP≤5; tPSA≤157; HBA≤10; HBD≤5; RB ≤ 15; Number of rings≤ 7; Number of carbons>4; Number of heteroatoms>1
- Veber (GSK) filter (Veber et al., 2002): RB≤10; tPSA≤140

In here, the filters generally state that an orally active drug should not violate the above criteria more than once. According to Table 2, it is observed that compound **7u** violates twice both Lipinski and Ghose filters. For all synthesized compounds except compound **7u**, it can be inferred that the rules of drug-likeness filters are followed. On the other hand, bioavailability score estimate the probability of a compound to have oral bioavailability in rat or measurable Caco-2 permeability and the bioavailability score value of a compound in the rat is expected to be >0.10 (Martin, 2005).A poor bioavailability results in lower activity of the molecule and higher inter-individual variability, and thus causes an unexpected response of a drug.The bioavailability score value of only compound **7u** is 0.17 and F values for all the synthesized compounds, co-ligand and melphalan are is 0.55. Log Kp presented in Table 2 is skin permeation parameter suggested by Potts (Potts and Guy 1992);high negative Log Kp value of the molecule indicates that the molecule has less penetration into the skin. Accordingly, it is observed that all the synthesized compounds have higher skin permeability than melphalan.

In summary, Table 2 shows the physicochemical properties, lipophilicity and water solubility values of the compounds used by various drug filters. When the violation values of the drug filter criteria are examined, as general trend, the synthesized compounds appears to be drug-likeness. Moreover, the favorable bioavailability scores of the synthesized compounds and the higher skin absorption relative to the reference drug relative to the LogKp values indicate that these compounds can be potential drug candidates.

Table 2. Pharmaceutical properties of compounds **7a-x**.

		Physicochemical Properties							Lipophilicity						Water Solubility		Violation of Drug-likeness filters						
Comp.	Binding Affinity	MW (g/mol)	Fsp^3	RB	HBA	HBD	MR	tPSA	iLogP	XLogP	WLogP	MLogP	SILICOS-IT	Consensus LogP	ESOL	Class	Lipinski	Ghose	Veber	Egan	Muegge	Bioavailability Score	Log K_p (cm/s)
7a	-10.9	408.45	0.08	6	4	1	122.45	69.04	3.36	3.76	3.57	3.18	4.18	3.61	-4.89	Moderately	0	0	0	0	0	0.55	-6.12
7b	-10.7	442.90	0.08	6	4	1	127.46	69.04	3.67	4.39	4.22	3.65	4.82	4.15	-5.49	Moderately	0	0	0	0	0	0.55	-5.88
7c	-11.1	422.48	0.12	6	4	1	127.41	69.04	3.54	4.12	3.87	3.38	4.71	3.93	-5.19	Moderately	0	0	0	0	0	0.55	-5.95
7d	-10.3	487.35	0.06	6	4	1	130.15	69.04	3.65	4.45	4.33	3.75	4.86	4.21	-5.80	Moderately	0	2	0	0	0	0.55	-6.11
7e	-11.0	442.90	0.08	6	4	1	127.46	69.04	3.71	4.39	4.22	3.65	4.82	4.16	-5.49	Moderately	0	0	0	0	0	0.55	-5.88
7f	-10.7	442.90	0.08	6	4	1	127.46	69.04	3.61	4.39	4.22	3.65	4.82	4.14	-5.49	Moderately	0	0	0	0	0	0.55	-5.88
7g	-10.9	487.89	0.08	7	6	1	136.28	114.86	3.35	4.22	4.13	3.58	2.65	3.59	-5.55	Moderately	0	2	0	0	0	0.55	-6.28
7h	-10.5	532.35	0.08	7	6	1	138.97	114.86	3.44	4.28	4.24	3.69	2.69	3.67	-5.86	Moderately	1	2	0	0	0	0.55	-6.51
7i	-10.8	487.89	0.08	7	6	1	136.28	114.86	3.16	4.22	4.13	3.58	2.65	3.55	-5.55	Moderately	0	2	0	0	0	0.55	-6.28
7j	-10.7	487.89	0.08	7	6	1	136.28	114.86	3.14	4.22	4.13	3.58	2.65	3.54	-5.55	Moderately	0	2	0	0	0	0.55	-6.28
7k	-10.6	453.45	0.08	7	6	1	131.27	114.86	3.08	3.59	3.47	3.11	2.01	3.05	-4.95	Moderately	0	1	0	0	0	0.55	-6.52
7l	-10.8	467.48	0.12	7	6	1	136.23	114.86	3.35	3.95	3.78	2.50	2.54	3.23	-5.25	Moderately	0	1	0	0	0	0.55	-6.35
7m	-10.9	422.48	0.12	6	4	1	127.41	69.04	3.60	4.12	3.87	3.38	4.71	3.94	-5.19	Moderately	0	0	0	0	0	0.55	-5.95
7n	-10.6	456.92	0.12	6	4	1	132.42	69.04	3.80	4.75	4.53	3.85	5.34	4.45	-5.79	Moderately	0	1	0	0	0	0.55	-5.71
7o	-11.5	436.51	0.15	6	4	1	132.38	69.04	3.70	4.49	4.18	3.59	5.23	4.24	-5.49	Moderately	0	1	0	0	0	0.55	-5.77
7p	-10.8	501.37	0.12	6	4	1	135.11	69.04	3.86	4.81	4.64	3.95	5.38	4.53	-6.10	Moderately	1	2	0	0	0	0.55	-5.94
7q	-10.9	456.92	0.12	6	4	1	132.42	69.04	3.92	4.75	4.53	3.85	5.34	4.48	-5.79	Moderately	0	1	0	0	0	0.55	-5.71
7r	-10.4	456.92	0.12	6	4	1	132.42	69.04	3.90	4.75	4.53	3.85	5.34	4.48	-5.79	Moderately	0	1	0	0	0	0.55	-5.71
7s	-10.7	442.90	0.08	6	4	1	127.46	69.04	3.62	4.39	4.22	3.65	4.82	4.14	-5.49	Moderately	0	0	0	0	0	0.55	-5.88
7t	-10.9	477.34	0.08	6	4	1	132.47	69.04	3.76	5.01	4.87	4.12	5.46	4.64	-6.08	Moderately	0	1	0	0	1	0.55	-5.65
7u	-10.8	521.79	0.08	6	4	1	135.16	69.04	3.88	5.08	4.98	4.22	5.49	4.73	-6.40	Moderately	2	2	0	0	1	0.17	-5.88
7v	-11.3	456.92	0.12	6	4	1	132.42	69.04	3.78	4.75	4.53	3.85	5.34	4.45	-5.79	Moderately	0	1	0	0	0	0.55	-5.71
7w	-11.0	477.34	0.08	6	4	1	132.47	69.04	3.81	5.01	4.87	4.12	5.46	4.65	-6.08	Moderately	0	1	0	0	1	0.55	-5.65
7x	-10.8	477.34	0.08	6	4	1	132.47	69.04	3.94	5.01	4.87	4.12	5.46	4.68	-6.08	Moderately	0	1	0	0	1	0.55	-5.65
Melphalan	-8.0	313.26	1.00	8	4	3	80.01	69.72	2.79	1.25	1.35	1.56	1.72	1.73	-2.04	Soluble	0	0	0	0	0	0.55	-7.32
Co-ligand	-8.1	364.55	1.00	2	4	2	99.73	35.50	0.00	4.01	2.95	3.49	1.02	2.29	-4.49	Moderately	0	0	0	0	0	0.55	-5.68

MW: molecular weight, Fsp^3:fraction of sp^3 carbon atoms, RB: rotatable bonds,HBD: hydrogen bonds donor, HBA: hydrogen bond acceptor, MR: molecular refractivity,tPSA: topological polar surface, LogP: indicator of lipophilicity,ESOL: solubility parameter, Log K_p: skin permeation.

Moreover, we depicted the bioavailability radar scheme in Figure 11 using SwissADMEwebserver. The bioavailability radar allows a rapid and more clear assessment of drug similarity of compounds. In the radar scheme, the red colored zone shows the suitable physicochemical space for oral bioavailability of molecules by taking into criteria such as flexibility, lipophilicity, saturation, size, polarity, and solubility. Validity limits of the criteria

are for Lipophilicity: -0.7<XLogP<+5.0, Size: 150<MW<500, Polar: 20<tPSA<130, Insolu: 0<ESOL<6, Insatu: 0.25<Fsp^3<1.00 and Flex: 0<RB<9. According to radar scheme, it is observed that all criteria except Insatu for all synthesized compounds remain within the red colored region. Lower Fsp3 values, in other words, the decrease of molecule saturation, is associated with lower solubility in water and this situation can be also seen from Table 2. It can be said that the oral bioavailability of the compounds synthesized according to the radar schemes is at an acceptable level.In summary, ADME predictions discussed in the paper shows that all synthesized compounds meet the criteria for being a possible drug candidate.

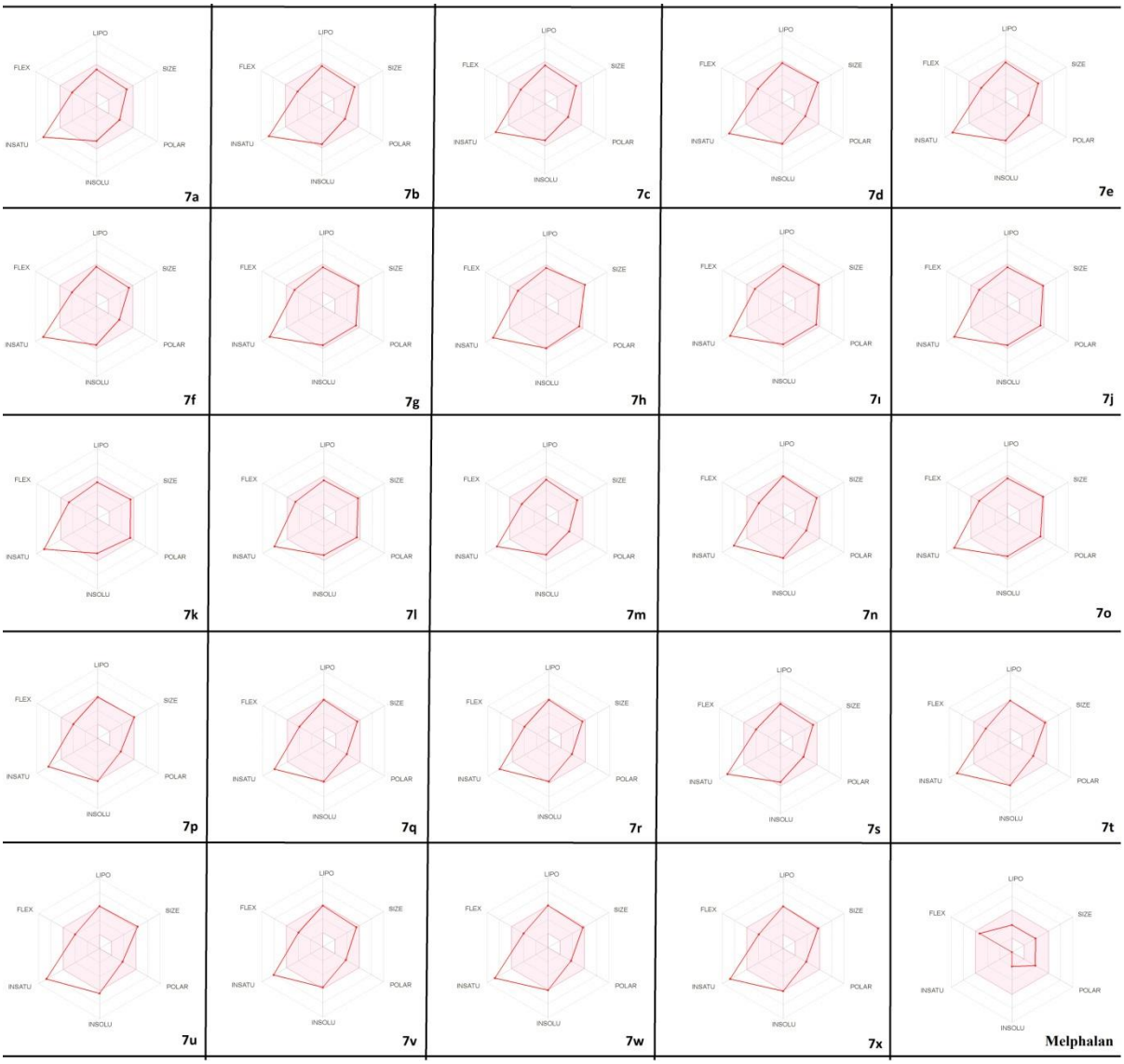

Figure 11. The bioavailability radar schemes of all synthesized compounds.

3.11. Molecular docking calculations

As mentioned before, EGFR is involved in the development of different cancer types. Therefore, the ability of potential new anticancer agents to target and eventually inhibit EGFR activityis considered an effective antitumor strategy, especially for solid tumors (Wykosky et al., 2011). For this reason, we also performed molecular docking simulations to identify the possible binding sites on the EGFR receptor. The highest binding affinity values obtained for all molecules were added to Table 2. It was observed that all compounds had higher docking scores than co-ligand (10-benzyl-2-fluoro-5,10-dihydro-11*H*-

dibenzo[*b*,*e*][1,4]diazepin-11-one), an inhibitor of the 6P8Q EGFR receptor. Therefore, it can be inferred that these compounds could act as EGFR inhibitors. When the values are examined, we also observe that docking affinity values are in good agreement with *in vitro* cytotoxicityresults. When the values are examined, it can be also observed that affinity values are in good agreement with the experimental activity results. The three compounds with the highest binding affinity are **7c** (-11.1 kcal/mol), **7o** (-11.5 kcal/mol) and **7v** (-11.3 kcal/mol) while the two compounds with the lowest binding affinity are compounds **7d** (-10.3 kcal/mol) and **7r** (-10.4 kcal/mol). Considering both these results and *in vitro* cytotoxicity results, we displayed the 2D interaction of these compounds and co-ligand with the 6P8Q EGFR receptor (Figure 12). It is seen in the diagram that all of the compounds **7c**, **7o**, and **7v** have, in common, hydrogen bond with MET793, Pi-Sulfur with MET790 and Pi-Alkyl type interactions with LEU788, ALA743. Therefore, it can be said that these residues play a key role for high binding affinity. On the other hand, compounds **7p** and **7r** with the lowest binding affinity have common eight interactions with the 6P8Q receptor. These interactions are Pi-Sigma with ALA726 and LEU 858, Ala743, LEU777, LEU788, Pi-Alky with MET790, Pi-Anion with ASP855, Pi-Sulfur with MET790. These common interactions could be an important finding for low binding affinity.

Due to the importance of hydrogen bonds in terms of the pharmacological properties of molecules, we also demonstrated the 3D interactions of the above-mentioned compounds and the co-ligand along with a hydrogen bond surface (Figure 13). From the figure, acceptor and donor surface areas can be seen easily.

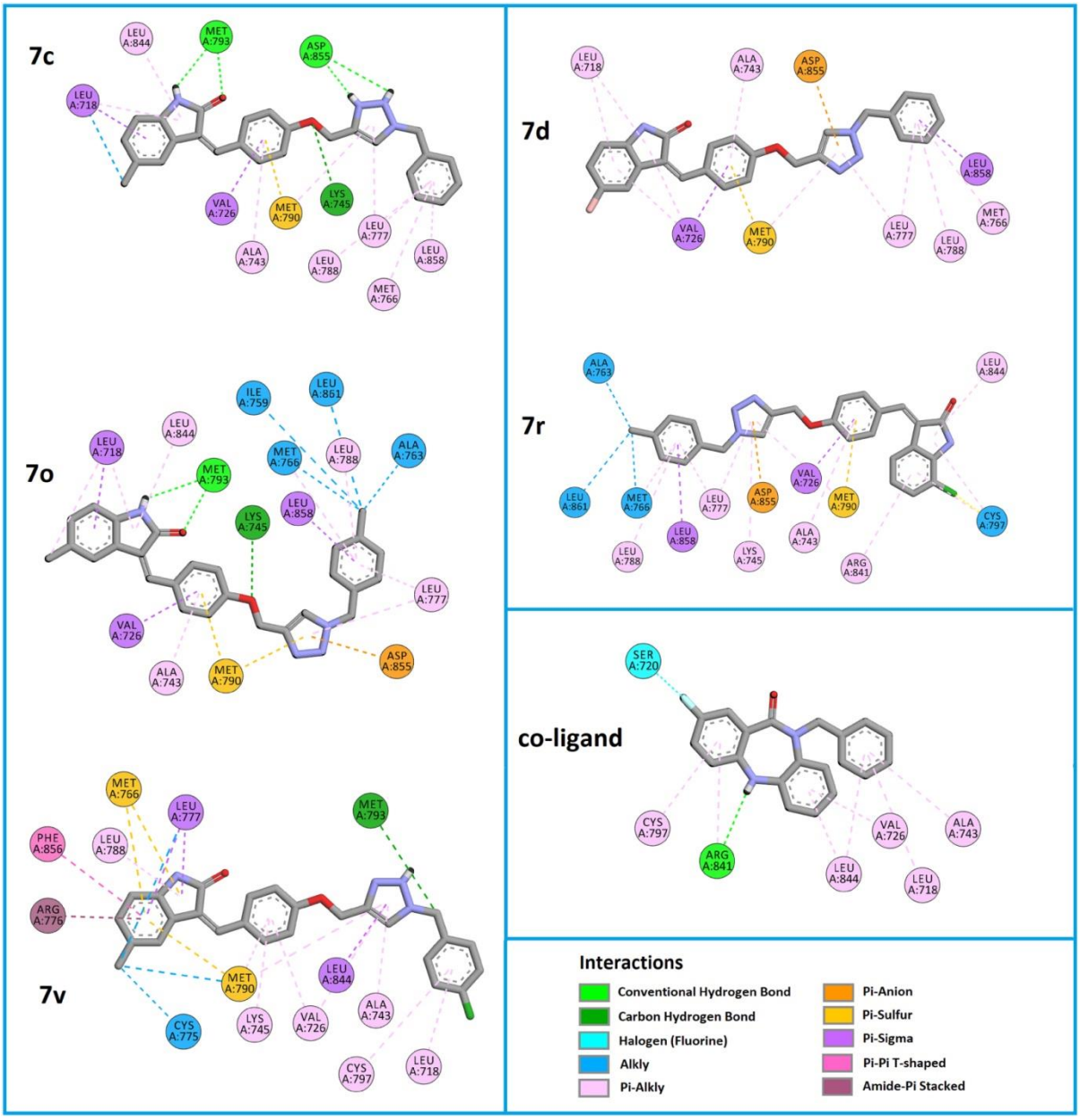

Figure 12.2D interaction diagram between 6P8Q receptor andcompounds**7c, 7d, 7o, 7r, 7v**, and co-ligand.

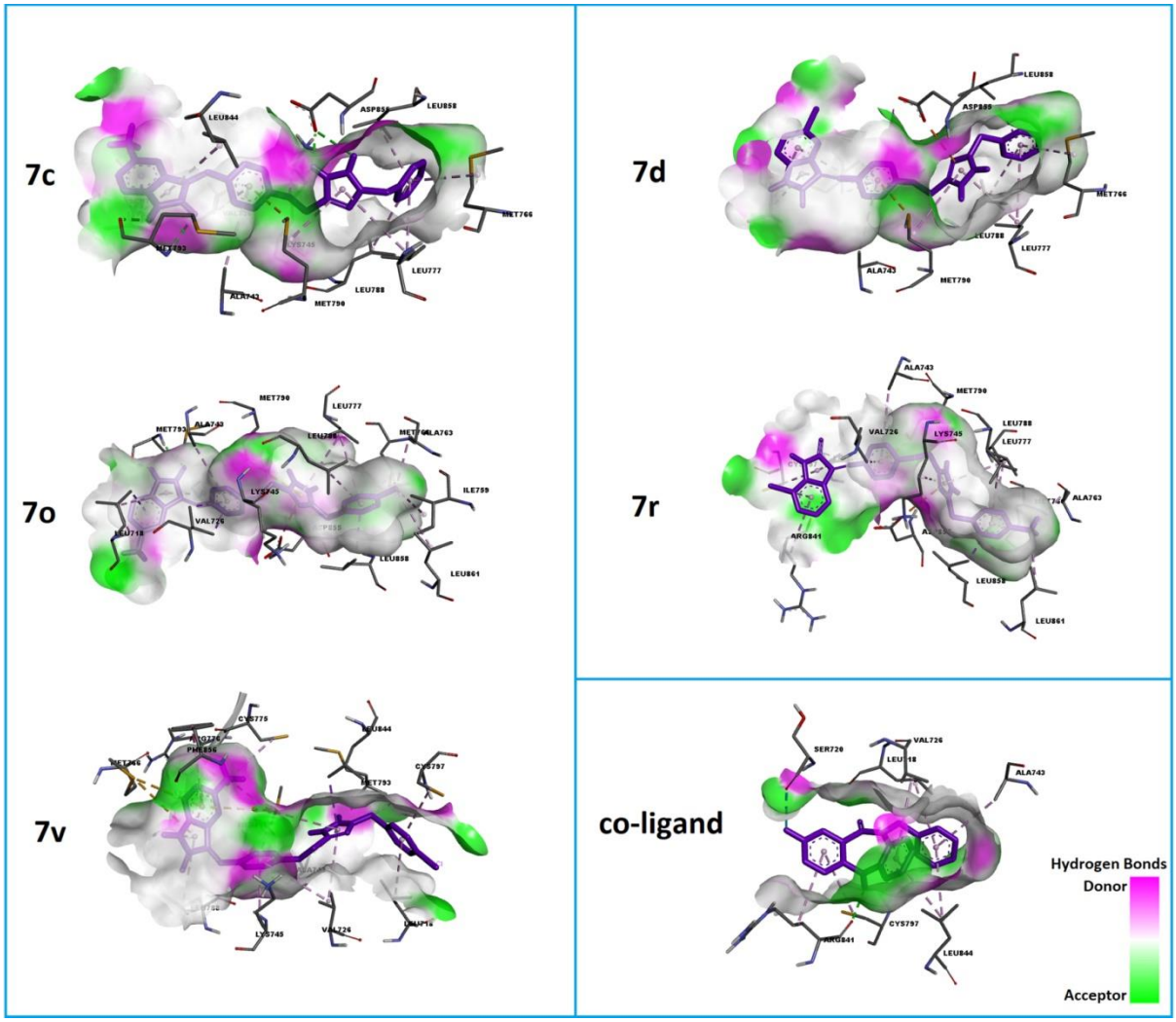

Figure 13.3D interactions on the Hydrogen Bond surface between 6P8Q receptor and compounds **7c**, **7d**, **7o**, **7r**, **7v**, and co-ligand.

4. Conclusion

A series of indolin-2-one linked 1,2,3-triazole derivatives **(7a-x)** was synthesized in good yield and evaluated for their cytotoxicity after due characterization. Most of the compounds were potent cytotoxic agents against CEM and HeLa cells with IC_{50} ranging from 1.5 to 67 µM and 3.4 to 133 µM respectively, whereas for L1210 cells, compounds **7a, 7c, 7o** and **7v** showed cytotoxicity between 3 to 8.1 µM. Compound**7c**was found to be equipotent with standard melphalan. Further studies carried out on Jurkat cells unveiled that **7c**induces apoptosis by activating both the intrinsic and the extrinsic apoptotic pathway. Thepro-apoptotic activity of **7c** showed to be closely associated with its ability to block the proliferation of cancer cells in the G2/M phase of cell cycle. Interestingly, compound **7c** did not show any genotoxic activity. In addition, the ADME properties of all the synthesized compounds were investigated and docking simulations were conducted to observe their inhibition effect on the 6P8Q EGFR receptor. The docking affinity results showed a good coherence with *in vitro cytotoxicity* results, observing also that all compounds possess higher docking scores compared with the co-ligand of 6P8Q EGFR receptor. As far as the potency

of compounds **7c**, **7o,** and **7v**is concerned, it was determined that the residues MET793, MET790, LEU788 and ALA743 of 6P8Q EGFR receptor had a key role.The ADME predictions showed that all synthesized compounds meet the criteria for being a possible drug candidate.Structure activity relationship study showed thatpresence of methyl group is preferred at position 5 of indolin-2-one against murine L1210 cells. Substitution made at position 5, 6 or 7 of indolin-2-one and position 4 of benzyl group increases the cytotoxic activity, against CEM cells. Replacement of hydrogen with -CH_3, -Cl and –NO_2 group on the position 4 of benzyl group improves cytotoxicity towards HeLa cells. In general, substitution on position 5, 6 or 7 of indoline-2-one increases cytotoxicity against HeLa cells.

Author Statement

AD and SK prepared the compounds, GG, and EC performed experiments to understand the mechanism of action, DS performed cytotoxicity study, RM, AL, and CF designed the in vitro experiments, HA, HT performed the in silico studies, FR performed cytotoxicity study against normal human cell line, SSK designed the scheme, interpreted the spectra, AD, SSK, and CF wrote the paper.

Acknowledgement

We would like to thank Agilent Technologies, Bengaluru (India) for LC-MS and NMR Research Centre-Indian Institute of Science, Bengaluru (India) for $^{1}H/^{13}C$-NMR spectral data.

Competing interest statement

The authors declare no conflict of interest

References

Akhter, M. H., Sateesh Madhav, N., Ahmad, J., 2018. Epidermal growth factor receptor based active targeting: a paradigm shift towards advance tumor therapy. Artif.Cells Nanomed. & Biotechnol. 46, 1188-1198. https://doi.org/10.1080/21691401.2018.1481863.

Amato, J., Iaccarino, N., Pagano, B., Morigi, R., Locatelli, A., Leoni, A., Rambaldi, M., Zizza, P., Biroccio, A., Novellino, E., & Randazzo, A., 2014. Bis-indole derivatives with antitumor activity turn out to be specific ligands of human telomeric G-quadruplex. Front. Chem. 2, 54. https://doi.org/10.3389/fchem.2014.00054.

Atulya N., Guntuku, L., Guggilapu, S. D., Danthi Bai K., Gannoju, S., Naidu, V.G.M., Bathini, N.B. 2016. Synthesis and apoptosis inducing studies of triazole linked 3-benzylidene isatin derivatives. Eur. J Med. Chem. 124, 782-793. https://doi.org/10.1016/j.ejmech.2016.09.009.

Baraldi, P.G., del Carmen Nunez, M., Tabrizi, M.A., De Clercq, E., Balzarini, J., Bermejo, J., Estévez, F., Romagnoli, R., 2004. Design, synthesis, and biological evaluation of hybrid molecules containing α-methylene-γ-butyrolactones and polypyrrole minor groove binders. J. Med. Chem., 47(11), 2877-2886. https://doi.org/10.1021/jm031104y.

Behbehani, H., Ibrahim, H.M., Makhseed, S., Mahmoud, H., 2011. Applications of 2-arylhydrazononitriles in synthesis: Preparation of new indole containing 1,2,3-triazole, pyrazole and pyrazolo[1,5-a]pyrimidine derivatives and evaluation of their antimicrobial activities. Eur. J. Med. Chem. 46(5), 1813-1820. https://doi.org/10.1016/j.ejmech.2011.02.040.

Behnisch-Cornwell, S., Bandaru, S.S.M., Napierkowski, M., Wolff, L., Zubair, M., Urbainsky, C., Lillig, C., Schulzke, C., Bednarski, P.J., 2020. Pentathiepins: A novel class of glutathione peroxidase 1 inhibitors that induce oxidative stress, loss of mitochondrial membrane potential and apoptosis in human cancer cells. ChemMedChem 15(16), 1515-1528. https://doi.org/10.1002/cmdc.202000160.

Biovia, D.S., 2017. Discovery studio modeling environment, San Diego: Dassault Systèmes.

Bonandi, E., Christodoulou, M.S., Fumagalli, G., Perdicchia, D., Rastelli, G., & Passarella, D., 2017. The 1,2,3-triazole ring as a bioisostere in medicinal chemistry, Drug Discov. Today 22(10), 1572-1581. https://doi.org/10.1016/j.drudis.2017.05.014.

Bradford, M.M., 1976. A rapid and sensitive method for the quantitation of microgram quantities of protein utilizing the principle of protein-dye binding. Anal. Biochem., 72(1), 248-254. https://doi.org/10.1016/0003-2697(76)90527-3.

Cao, J.Y., Dixon, S.J., 2016. Mechanisms of ferroptosis. Cell Mol. Life Sci. 73(11), 2195-2209. https://doi.org/10.1007/s00018-016-2194-1.

Carroux, C.J., Rankin, G.M., Moeker, J., Bornaghi, L.F. Katneni, K., Morizzi, J., Charman, S.A., Vullo, D., Supuran, C.T., Poulsen, S.-A., 2013. A prodrug approach toward cancer-related carbonic anhydrase inhibition. J. Med. Chem. 56(23), 9623-9634. https://doi.org/10.1021/jm401163e.

Chen, J., Kos, R., Garssen, J., Redegeld, F., 2019. Molecular insights into the mechanism of necroptosis: the necrosome as a potential therapeutic target. Cells 8(12), 1486. https://doi.org/10.3390/cells8121486

Chen, M., Lu, S., Yuan, G., Yang, S., Du, X., 2000. Synthesis and antibacterial activity of some heterocyclic β-enamino ester derivatives with 1,2,3-triazole. Heterocycl. Commun. 6 (5), 421-426. https://doi.org/10.1515/HC.2000.6.5.421.

Chen, Y., Lopez-Sanchez, M., Savoy, D.N., Billadeau, D.D., Dow, G.S., Kozikowski, A.P. 2008. A series of potent and selective, triazolylphenyl-based histone deacetylases inhibitors with activity against pancreatic cancer cells and plasmodium falciparum. J. Med. Chem.51(12), 3437-3448. doi.org/10.1021/jm701606b

Daina, A., Michielin, O., Zoete, V., 2014. iLOGP: a simple, robust, and efficient description of n-octanol/water partition coefficient for drug design using the GB/SA approach. J. Chem. Inf. Model. 54(12), 3284-3301. https://doi.org/10.1021/ci500467k.

Daina, A., Michielin, O., Zoete, V., 2017. SwissADME: a free web tool to evaluate pharmacokinetics, drug-likeness and medicinal chemistry friendliness of small molecules. Sci. Rep. 7, 42717. https://doi.org/10.1038/srep42717.

Dallakyan, S., & Olson, A.J., 2015. Small-molecule library screening by docking with PyRx, Chemical biology, Springer, pp. 243-250. https://doi.org/10.1007/978-1-4939-2269-7_19.

D'Arcy, M.S., 2019. Cell death: a review of the major forms of apoptosis, necrosis and autophagy. Cell Biol. Int. 43(6), 582-592. https://doi.org/10.1002/cbin.11137.

Das, A., Kumar, S., Persoons, L., Daelemans, D., Schols, D., Alici, H., Tahtaci, H., Karki, S.S., 2021. Synthesis, in silico ADME, molecular docking and in vitro cytotoxicity evaluation of stilbene linked 1,2,3-triazoles. Heliyon 7(1), e05893. doi: 10.1016/j.heliyon.2020.e05893.

De Clercq, D.J.H., Heppner, D.E., To, C., Jang, J., Park, E., …..D.A. Scott., 2019. Discovery and optimization of dibenzodiazepinones as allosteric mutant-selective EGFR inhibitors. ACSMed.Chem. Lett. 10(11), 1549-1553. https://doi.org/10.1021/acsmedchemlett.9b00381

Delaney, J.S., 2004. ESOL: estimating aqueous solubility directly from molecular structure. J. Chem. Inf. Model. 44(3), 1000-1005. https://doi.org/10.1021/ci034243x.

Duan, Y.-C., Ma, Y.-C. Zhang, E., Shi, X.-J., Wang, M.-M., Ye, X.-W., Liu, H.-M., 2013. Design and synthesis of novel 1,2,3-triazole-dithiocarbamate hybrids as potential anticancer agents. Eur. J. Med. Chem.62, 11-19. https://doi.org/10.1016/j.ejmech.2012.12.046.

Egan, W.J., Merz, K.M., Baldwin, J.J., 2000. Prediction of drug absorption using multivariate statistics. J. Med. Chem. 43(21), 3867-3877. https://doi.org/10.1021/jm000292e.

Erol, D. D., Çaliş, Ü., Demirdamar, R., Yuluğ, N., Ertan, M., 1995. Synthesis and biological activities of some 3,6-disubstituted thiazolo[3,2-b][1,2,4]triazoles. J. Pharm. Sci. 84(4), 462-465. https://doi.org/10.1002/jps.2600840414

Fulda, S., 2009. Tumor resistance to apoptosis. Int. J. Cancer 124(3), 511-515. https://doi.org/10.1002/ijc.24064.

Galluzzi, L., Vitale, I., Aaronson, S.A., Abrams, J.M., Adam, D., Agostinis, P., Alnemri, E.S., Altucci, L., ……Kroemer, G., 2018. Molecular mechanisms of cell death: recommendations of the nomenclature committee on cell death. Cell Death and Differentiation 25(3), 486-541. https://doi.org/10.1038/s41418-017-0012-4.

Ghose, A.K., Viswanadhan, V.N., Wendoloski, J.J., 1999. A knowledge-based approach in designing combinatorial or medicinal chemistry libraries for drug discovery. 1. A qualitative and quantitative characterization of known drug databases. J. Comb. Chem. 1 (1), 55-68. https://doi.org/10.1021/cc9800071.

Giulia, G., Eleonora, T., Massimo, T., Immacolata, M., Carmela, F., 2021. The alcoholic bark extract of terminalia arjuna exhibits cytotoxic and cytostatic activity on jurkat leukemia cells. Venoms and Toxins 1, 1-11. http://doi.org/10.2174/2666121701999200601170928.

Grandis, J.R. , Melhem, M.F., Gooding, W.E., Day, R., Holst, V.A., Wagener, M.M., Drenning, S.D., Tweardy, D.J., 1998. Levels of TGF-α and EGFR protein in head and neck squamous cell carcinoma and patient survival. J. Nat. Cancer Inst.90(11), 824-832. https://doi.org/10.1093/jnci/90.11.824.

Gujjar, R., Marwaha, A., El Mazouni, F., White, J., White, K.L., Creason, S., Shackleford, D.M., Baldwin, J., Charman, W.N., Buckner, F.S., Charman, S., Rathod, P.K., Phillips, M.A., 2009. Identification of a metabolically stable triazolopyrimidine-based dihydroorotate dehydrogenase inhibitor with antimalarial activity in mice, J. Med. Chem. 52(7), 1864-1872. https://doi.org/10.1021/jm801343r.

Hafez, H., Abbas, H.-A., El-Gazzar, A.-R., 2008. Synthesis and evaluation of analgesic, anti-inflammatory and ulcerogenic activities of some triazolo- and 2-pyrazolyl-pyrido[2,3-d]-pyrimidines. Acta Pharm. 58(4), 359-378. https://doi.org/10.2478/v10007-008-0024-1.

Hanwell, M.D., Curtis, D.E., Lonie, D.C., Vandermeersch, T., Zurek, E., Hutchison, G.R., 2012. Avogadro: an advanced semantic chemical editor, visualization, and analysis platform. J. Cheminform. 4(1), 17. https://doi.org/10.1186/1758-2946-4-17.

Hochegger, H., Takeda, S., Hunt, T., 2008. Cyclin-dependent kinases and cell-cycle transitions: does one fit all?, Nat. Rev. Mol. Cell Biol. 9(11), 910-916. https://doi.org/10.1038/nrm2510.

Holla, B.S., Mahalinga, M., Karthikeyan, M.S., Poojary, B., Akberali, P.M., Kumari, N.S. 2005, Synthesis, characterization and antimicrobial activity of some substituted 1,2,3-triazoles. Eur. J. Med. Chem. 40(11), 1173-1178. https://doi.org/10.1016/j.ejmech.2005.02.013.

Hong, L., Lin, W., Zhang, F., Liu, R., Zhou, X., 2013. Ln[$N(SiMe_3)_2$]$_3$-catalyzed cycloaddition of terminal alkynes to azides leading to 1,5-disubstituted 1,2,3-triazoles: new mechanistic features. Chem. Commun.49, 5589-5591. https://doi.org/10.1039/C3CC42534G.

Hussain, M., Qadri, T., Hussain, Z., Saeed, A., Channar, P.A., Shehzadi, S.A., Hassan, M., Larik, F.A., Mahmood, T., Malik, A., 2019. Synthesis, antibacterial activity and molecular docking study of vanillin derived 1,4-disubstituted 1,2,3-triazoles as inhibitors of bacterial DNA synthesis. Heliyon 5 (11), E02812. https://doi.org/10.1016/j.heliyon.2019.e02812

Huey, R., Morris, G.M., Olson, A.J., Goodsell, D.S., 2007. A semiempirical free energy force field with charge-based desolvation. J. Comput. Chem. 28(6), 1145-1152. https://doi.org/10.1002/jcc.20634.

Iyer, D., Vartak, S.V., Mishra, A., Goldsmith, G., Kumar, S., Srivastava, M., Hegde, M., Gopalakrishnan, V., Glenn, M., Velusamy, M., Choudhary, B., Kalakonda, N., Karki, S.S., Surolia, A., Raghavan, S. C., 2016. Identification of a novel BCL2-specific inhibitor that binds predominantly to the BH1 domain. FEBS J. 283(18), 3408-3437. https://doi.org/10.1111/febs.13815.

Jain, P., Singh, V., Ali,S., Tripathi, V., Saraswat, U., 2018.Synthesis, characterization, molecular docking and biological activity of 5,6-bis-(4-fluoro-phenyl)-3,4,7,8-tetraaza-bicyclo[8.3.1]tetradeca-1(13) 4,6,10(14),11-pentaene-2,9-dione and its transition metal complexes. J. Saudi Chem. Soc. 22(5), 546-557. https://doi.org/10.1016/j.jscs.2017.09.005

Jia, Y., Wen, X., Gong, Y., Wang, X., 2020. Current scenario of indole derivatives with potential anti-drug-resistant cancer activity. Eur. J. Med. Chem. 200, 112359. https://doi.org/10.1016/j.ejmech.2020.112359

Johns, B.A., Weatherhead, J.G., Allen, S.H., Thompson, J.B., Garvey, E.P., Foster, S.A., Jeffrey, J.L., Miller, W.H., 2009. 1,3,4-oxadiazole substituted naphthyridines as HIV-1 integrase inhibitors. part 2: SAR of the C5 position. Bioorg. Med. Chem. Lett. 19(6), 1807-1810. https://doi.org/10.1016/j.bmcl.2009.01.089.

Kalyankrishna, S., Grandis, J.R., 2006. Epidermal growth factor receptor biology in head and neck cancer. J. Clin. Oncol. 24(17), 2666-2672. https://doi.org/10.1200/JCO.2005.04.8306.

Kilic-Kurt, Z., Acar, C., Ergul, M., Bakar-Ates, F., Altuntas, T.G., 2020. Novel indole hydrazide derivatives: Synthesis and their antiproliferative activities through inducing apoptosis and DNA damage. Arch. Pharm. 353(8), 2000059. https://doi.org/10.1002/ardp.202000059.

Kumar, D., Beena, Khare, G., Kidwai, S., Tyagi, A.K., Singh, R., Rawat, D.S., 2014. Synthesis of novel 1,2,3-triazole derivatives of isoniazid and their in vitro and in vivo antimycobacterial activity evaluation. Eur. J. Med. Chem. 81, 301-313. https://doi.org/10.1016/j.ejmech.2014.05.005.

Kumar, R., Arora, J., Prasad A.K., Islam, N., Verma, A.K., 2013. Synthesis and antimicrobial activity of pyrimidine chalcones. Med. Chem. Res., 22, 5624-5631.https://doi.org/10.1007/s00044-013-0555-y.

Lipinski, C.A., Lombardo, F., Dominy, B.W., Feeney, P.J., 1997. Experimental and computational approaches to estimate solubility and permeability in drug discovery and development settings. Adv. Drug. Deliv. Rev. 23(1-3), 3-25. https://doi.org/10.1016/s0169-409x(00)00129-0.

Martin, Y.C., 2005. A bioavailability score. J. Med. Chem. 48(9), 3164-3170. https://doi.org/10.1021/jm0492002.

Lovering, F., Bikker, J., Humblet, C., 2009. Escape from flatland: increasing saturation as an approach to improving clinical success. J. Med. Chem. 52(21), 6752-6756. https://doi.org/10.1021/jm901241e.

Mady, M.F., Awad, G.E.A., Jørgensen, K.B., 2014. Ultrasound-assisted synthesis of novel 1,2,3-triazoles coupled diaryl sulfone moieties by the CuAAC reaction, and biological

evaluation of them as antioxidant and antimicrobial agents. Eur. J. Med. Chem.84, 433-443. https://doi.org/10.1016/j.ejmech.2014.07.042.

Mah, L.J., El-Osta, A., Karagiannis, T.C., 2010. γH2AX: a sensitive molecular marker of DNA damage and repair. Leukemia 24(4), 679-686. https://doi.org/10.1038/leu.2010.6.

Mellinghoff, I.K., Wang, M.Y., Vivanco, I., Haas-Kogan, D.A., Zhu, S., Dia, E.Q., Lu, K.V., Yoshimoto, K., Huang, J.H.Y., Chute, D.J.,……Mischel. P.S.,2005. Molecular determinants of the response of glioblastomas to EGFR kinase inhibitors, N. Engl. J. Med. 353(19), 2012-2024. https://doi.org/10.1056/NEJMoa051918.

Mitsudomi, T., Yatabe, Y., 2010. Epidermal growth factor receptor in relation to tumor development: EGFR gene and cancer. FEBS J. 277(2), 301-308. https://doi.org/10.1111/j.1742-4658.2009.07448.x.

Mohammad, R.M., Muqbil, I., Lowe, L., Yedjou, C., ……..Azmi, A.S., 2015. Broad targeting of resistance to apoptosis in cancer. Semin. Cancer Biol. 35, S78-S103. https://doi.org/10.1016/j.semcancer.2015.03.001.

Morrison, J., Haldar, K., Kehoe, S., Lawrie, T.A., 2012. Chemotherapy versus surgery for initial treatment in advanced ovarian epithelial cancer, Cochrane Database Syst. Rev. 8, CD005343. https://doi.org/10.1002/14651858.CD005343.pub3.

Nagata, S., 2018. Apoptosis and clearance of apoptotic cells. Annu. Rev. Immunol. 36(1), 489-517. https://doi.org/10.1146/annurev-immunol-042617-053010.

Narsimha, S., Satheesh, K. N., Kumara, S. B., Reddy, N.V., Althaf Hussain, S.K., Rao, M. S., 2016. Indole-2-carboxylic acid derived mono and bis 1,4-disubstituted 1,2,3-triazoles: Synthesis, characterization and evaluation of anticancer, antibacterial, and DNA-cleavage activities. Bioorg. Med. Chem. Lett. 26(6), 1639-1644. https://doi.org/10.1016/j.bmcl.2016.01.055

Nielsen, J.S., Jakobsen, E., Holund, B., Bertelsen, K., Jakobsen, A., 2004. Prognostic significance of p53, Her-2, and EGFR overexpression in borderline and epithelial ovarian cancer. Int. J. Gynecol. Cancer 14(6), 1086-1096. https://doi.org/10.1111/j.1048-891X.2004.14606.x.

Muegge, I., Heald, S.L., Brittelli, D., 2001. Simple selection criteria for drug-like chemical matter. J. Med. Chem. 44(12), 1841-1846. https://doi.org/10.1021/jm015507e.

Nohmi, T., 2018. Thresholds of genotoxic and non-genotoxic carcinogens. Toxicol. Res. 34(4), 281-290. https://doi.org/10.5487/TR.2018.34.4.281

Patpi, S.R., Pulipati, L., Yogeeswari, P., Sriram, D., Jain, N., Sridhar, B., Murthy, R., Anjana, D. T, Kalivendi, S.V., Kantevari, S., 2012. Design, Synthesis, and structure–activity correlations of novel dibenzo[b,d]furan, dibenzo[b,d]thiophene, and n-methylcarbazole clubbed 1,2,3-triazoles as potent inhibitors of mycobacterium tuberculosis. J. Med. Chem. 55(8), 3911-3922. https://doi.org/10.1021/jm300125e.

Pearce, S., 2017. The importance of heterocyclic compounds in anti-cancer drug design. 66 Available online: https://www.ddw-online.com/therapeutics/p320375-the-importance-of-heterocyclic%20compounds-in-anti-cancer-drug-design.html

Potts, R.O., Guy, R.H. 1992. Predicting skin permeability. Pharm. Res. 9(5), 663-669. https://doi.org/10.1023/a:1015810312465.

Qin, X., Ma, D., Tan, Y.-x., Wang, H.-y., Cai, Z., 2019. The role of necroptosis in cancer: A double-edged sword?, Biochim. Biophys. Acta Rev. Cancer 1871(2), 259-266. https://doi.org/10.1016/j.bbcan.2019.01.006

Rao, P. S., Kurumurthy, C., Veeraswamy, B., Santhosh Kumar, G., Poornachandra, Y., Ganesh Kumar, C., Vasamsetti, S.B., Kotamraju, S., Narsaiah, B., 2014. Synthesis of novel 1,2,3-triazole substituted-N-alkyl/aryl nitrone derivatives, their anti-inflammatory and anticancer activity, Eur. J. Med. Chem. 80, 184-191. https://doi.org/10.1016/j.ejmech.2014.04.052.

Sheehan, D.J., Hitchcock, C.A., Sibley, C.M., 1999. Current and emerging azole antifungal agents, Clin. Microbiol. Rev. 12(1), 40-79. https://doi.org/10.1128/CMR.12.1.40.

Sigismund, S., Avanzato, D., Lanzetti, L., 2018. Emerging functions of the EGFR in cancer, Mol. Oncol.12(1), 3-20. https://doi.org/10.1002/1878-0261.12155.

Solis, F.J., Wets, R.J.-B., 1981. Minimization by random search techniques. Math. Oper. Res. 6(1), 19-30. https://doi.org/10.1287/moor.6.1.19.

Soriano, D.S., 1993. Example of the Wolff-Kishner reduction procedure suitable for an undergraduate organic lab experiment: Preparation of oxindole. J. Chem. Educ. 70(4), 332. https://doi.org/10.1021/ed070p332.

Sztanke, K., Pasternak, K., Rzymowska, J., Sztanke, M., Kandefer-Szerszeń, M., 2008. Synthesis, structure elucidation and identification of antitumoural properties of novel fused 1,2,4-triazine aryl derivatives, Eur. J. Med. Chem. 43(5), 1085-1094. https://doi.org/10.1016/j.ejmech.2007.07.009.

Sujeet K., Mahesh H., Vidya G., Vinaya K.R., Sureshbabu A.R., Erik De C., Dominique S., Anil K.G.N., Sathees C.R., Subhas S. K., 2014. 2-(4-Chlorobenzyl)-6-arylimidazo[2,1-b][1,3,4]thiadiazoles: Synthesis, cytotoxic activity and mechanism of action, Eur. J. Med. Chem. 84, 687-697. https://doi.org/10.1016/j.ejmech.2014.07.054.

Tait, S.W.G., Ichim, G., Green, D.R., 2014. Die another way – non-apoptotic mechanisms of cell death. J. Cell Sci. 127(10), 2135. https://doi.org/doi:10.1242/jcs.093575.

To, C., Jang, J., Chen, T., Park, E., Mushajiang, M., De Clercq, D.J.H., …..Janne, P.A., 2019. Single and dual targeting of mutant Egfr with an allosteric inhibitor, Cancer Discov., 9(7), 926-943. https://doi.org/10.1158/2159-8290.CD-18-0903.

Trott, O., Olson, A.J., 2010. AutoDock Vina: improving the speed and accuracy of docking with a new scoring function, efficient optimization, and multithreading. J. Comput. Chem. 31(2), 455-461. https://doi.org/10.1002/jcc.21334.

Ulloora, S., Shabaraya, R., Adhikari, A.V., 2013. Facile synthesis of new imidazo[1,2-a]pyridines carrying 1,2,3-triazoles via click chemistry and their antiepileptic studies. Bioorg. Med. Chem. Lett. 23(11), 3368-3372. https://doi.org/10.1016/j.bmcl.2013.03.086.

Veber, D.F., Johnson, S.R., Cheng, H.-Y., Smith, B.R. , Ward, K.W., Kopple, K.D., 2002. Molecular properties that influence the oral bioavailability of drug candidates. J. Med. Chem. 45(12), 2615-2623. https://doi.org/10.1021/jm020017n.

Velázquez, S., Alvarez, R., Pérez, C., Gago, F., De Clercq, E., Balzarini, J., Camarasa, M.J., 1998. Regiospecific synthesis and anti-human immunodeficiency virus activity of novel 5-substituted n-alkylcarbamoyl and n,n-dialkyl carbamoyl 1,2,3-triazole-TSAO analogues. Antiviral Chem. Chemother. 9(6), 481-489. https://doi.org/10.1177/095632029800900604.

Verhaak, R.G., Hoadley, K.A., Purdom, E., Wang, V., Qi, Y., Wilkerson, M.D., Miller, C.R., Ding, L., Golub, T., Mesirov, J.P., Alexe, G., Lawrence, M., O'Kelly, M., ….HayesD.N., 2010. Cancer Genome Atlas Research, Integrated genomic analysis identifies clinically relevant subtypes of glioblastoma characterized by abnormalities in PDGFRA, IDH1, EGFR, and NF1. Cancer Cell 17(1), 98-110. https://doi.org/10.1016/j.ccr.2009.12.020.

Walker, F., Abramowitz, L., Benabderrahmane, D., Duval, X., Descatoire, V., Henin, D., Lehy, T., Aparicio, T., 2009. Growth factor receptor expression in anal squamous lesions: modifications associated with oncogenic human papillomavirus and human immunodeficiency virus. Hum. Pathol. 40(11), 1517-1527. https://doi.org/10.1016/j.humpath.2009.05.010.

Wan, Y., Li, Y., Yan, C., Yan, M., Tang, Z., 2019. Indole: A privileged scaffold for the design of anti-cancer agents. Eur. J. Med. Chem. 183, 111691. https://doi.org/10.1016/j.ejmech.2019.111691.

Wykosky, J., Fenton, T., Furnari, F., Cavenee, W.K., 2011. Therapeutic targeting of epidermal growth factor receptor in human cancer: successes and limitations. Chin. J. Cancer 30(1), 5-12. https://doi.org/10.5732/cjc.010.10542.

Yan, S.-J., Liu, Y.-J., Chen, Y.-L., Liu, L., Lin, J., 2010. An efficient one-pot synthesis of heterocycle-fused 1,2,3-triazole derivatives as anti-cancer agents. Bioorg. Med. Chem. Lett.20(17), 5225-5228. https://doi.org/10.1016/j.bmcl.2010.06.141.

Yempala, T., Sridevi, J.P., Yogeeswari, P., Sriram, D., Kantevari, S., 2014. Rational design and synthesis of novel dibenzo[b,d]furan-1,2,3-triazole conjugates as potent inhibitors of mycobacterium tuberculosis. Eur. J. Med. Chem. 71, 160-167. https://doi.org/10.1016/j.ejmech.2013.10.082.

Zimmermann, M., Meyer, N., 2011. Annexin V/7-AAD Staining in Keratinocytes, in: M.J. Stoddart (Ed.) Mammalian Cell Viability: Methods and Protocols, Humana Press, Totowa, NJ, pp. 57-63. https://doi.org/10.1007/978-1-61779-108-6_8.